

5-2010

## **An improved wideband Vivaldi antenna design**

Fang Chen  
*University of Texas-Pan American*

Follow this and additional works at: [https://scholarworks.utrgv.edu/leg\\_etd](https://scholarworks.utrgv.edu/leg_etd)



Part of the [Electrical and Computer Engineering Commons](#)

---

### **Recommended Citation**

Chen, Fang, "An improved wideband Vivaldi antenna design" (2010). *Theses and Dissertations - UTB/UTPA*. 170.

[https://scholarworks.utrgv.edu/leg\\_etd/170](https://scholarworks.utrgv.edu/leg_etd/170)

This Thesis is brought to you for free and open access by ScholarWorks @ UTRGV. It has been accepted for inclusion in Theses and Dissertations - UTB/UTPA by an authorized administrator of ScholarWorks @ UTRGV. For more information, please contact [justin.white@utrgv.edu](mailto:justin.white@utrgv.edu), [william.flores01@utrgv.edu](mailto:william.flores01@utrgv.edu).

AN IMPROVED WIDEBAND  
VIVALDI ANTENNA DESIGN

A Thesis

by

FANG CHEN

Submitted to the Graduate School of the  
University of Texas Pan-American  
In partial fulfillment of the requirements for the Degree of

MASTER OF SCIENCE

May 2010

Major Subject: Electrical Engineering

AN IMPROVED WIDEBAND  
VIVALDI ANTENNA DESIGN

A Thesis  
by  
FANG CHEN

COMMITTEE MEMBERS

Dr. Junfei Li  
Chair of Committee

Dr. Heinrich Foltz  
Committee Member

Dr. Jae Sok Son  
Committee Member

May 2010

Copyright 2010 Fang Chen

All Rights Reserved

## ABSTRACT

Chen Fang, An Improved Wideband Vivaldi Antenna Design. Master of Science (MS), May, 2010, 58 pp., 2 tables, 35 figures, references, 38 titles.

The objectives of this thesis are to 1) determine how Vivaldi antenna parameters affect the performance and 2) design a Vivaldi antenna with improved overall performance over existing designs.

The methodology is to divide the Vivaldi antenna into two parts consisting of microstrip-to-slotline transition and tapered curve part. This has great advantages in finding the relationships between the different antenna parameters and the antenna performance. By combining the methods of improving the impedance- and usable gain bandwidth concluded by the parameter study on the two individual parts, a final Vivaldi antenna design with 10:1 bandwidth is achieved in terms of both types of bandwidth.

Measurements from the fabricated Vivaldi antenna show good agreements with the CST simulation results in terms of reflection coefficient, gain and impulse response.

## ACKNOWLEDGEMENTS

I am delighted to take this opportunity to express the sincere thanks to my advisor, Dr. Junfei Li, for his guidance and support during the two-year research time. His research ideas, advice, valuable lessons during my research have made a significant contribution to this thesis.

I would also like to extend my gratitude to Dr. Heinrich Foltz for not only serving on my committee, but also for the invaluable time and effort that he has put into this research. I would like to acknowledge that without his advice this project would not have been completed in time.

I also take this opportunity to thank Dr. Jae Sok Son for always being willing to answer my questions about the thesis research and course study. I also appreciate his suggestions for my ph.D application.

Special thanks go to my family members. Their unconditional love, moral support and continuous encouragement enable to accomplish all that I have.

Thanks to Xiaohui Wang and Yu Bai for their help in my study life. Thanks to all my friends at UTPA who have made my stay in a pleasant and memorable one.

The research was partially supported by ARO W911NF0610420, AFOSR/ARO W911NF0810511 and NSF 0421352. Thanks to those grants support.

## TABLE OF CONTENTS

|   | Page |
|---|------|
| ABSTRACT.....                               | iii  |
| ACKNOWLEDGEMENTS.....                       | iv   |
| TABLE OF CONTENTS.....                      | v    |
| LIST OF TABLES.....                         | viii |
| LIST OF FIGURES .....                       | ix   |
| CHAPTER I. INTRODUCTION.....                | 1    |
| 1.1 Background.....                         | 1    |
| 1.2 Current research.....                   | 1    |
| 1.3 Objective.....                          | 2    |
| 1.4 Organization.....                       | 2    |
| CHAPTER II. VIVALDI ANTENNA.....            | 4    |
| 2.1 Taper types of TSA.....                 | 4    |
| 2.2 Principle of Vivaldi antenna .....      | 5    |
| 2.3 Feeding techniques .....                | 7    |
| 2.4 Method of approach .....                | 8    |
| 2.4.1 Multi-objective.....                  | 9    |
| 2.4.2 Multiple simulation tools .....       | 10   |
| 2.4.3 Division into two parts.....          | 14   |
| CHAPTER III. RESEARCH ON TAPER PROFILE..... | 18   |
| 3.1 Exponential taper .....                 | 18   |

|   |    |
|---|----|
| 3.1.1 Taper stepline model.....               | 18 |
| 3.1.2 Tapered transmission line .....         | 19 |
| 3.2 Parameter effect .....                    | 20 |
| 3.2.1 Substrate size .....                    | 20 |
| 3.2.2 Substrate dielectric constant .....     | 21 |
| 3.2.3 Substrate thickness.....                | 22 |
| 3.2.4 Curvature profile.....                  | 22 |
| 3.3 Conclusion .....                          | 24 |
| CHAPTER IV. RESEARCH ON TRANSITION PART ..... | 26 |
| 4.1 Transition types.....                     | 26 |
| 4.2 Equivalent circuit .....                  | 27 |
| 4.3 Traditional parameter design .....        | 29 |
| 4.4 Novel parameter design .....              | 31 |
| 4.5 Parameter sweep .....                     | 35 |
| 4.6 Conclusion .....                          | 36 |
| CHAPTER V. FINAL VIVALDI ANTENNA DESIGN.....  | 37 |
| 5.1 Design parameters.....                    | 37 |
| 5.2 CST simulation results.....               | 40 |
| 5.2.1 Impedance bandwidth .....               | 40 |
| 5.2.2 E field.....                            | 41 |
| 5.2.3 Radiation pattern.....                  | 43 |
| 5.2.4 Gain bandwidth.....                     | 44 |
| 5.2.5 Impulse response.....                   | 45 |
| CHAPTER VI. VIVALDI ANTENNA MEASUREMENT.....  | 47 |
| 6.1 Test setup .....                          | 47 |
| 6.2 Reflection measurement .....              | 48 |

|  |    |
|--|----|
| 6.3 Gain measurement .....                     | 48 |
| 6.4 Impulse response measurement .....         | 50 |
| CHAPTER VII. CONCLUSION AND CONTRIBUTION ..... | 52 |
| 7.1 Conclusion .....                           | 52 |
| 7.2 Contribution .....                         | 52 |
| REFERENCES .....                               | 54 |
| BIOGRAPHICAL SKETCH .....                      | 58 |

## LIST OF TABLES

|   | Page |
|---|------|
| Table 2.1: Bandwidth indicators and related quantitative standards..... | 10   |
| Table 5.1: Simulation settings in CST MWS.....                          | 40   |

## LIST OF FIGURES

|  | Page |
|--|------|
| Figure 2.1: Different taper-styles of the TSA.....                             | 4    |
| Figure 2.2: Typical radiation pattern of TSA.....                              | 6    |
| Figure 2.3: Vivaldi antenna taper structure .....                              | 6    |
| Figure 2.4: Microstrip to slotline transition.....                             | 7    |
| Figure 2.5: Vivaldi antenna configuration.....                                 | 12   |
| Figure 2.6: CST and HFSS simulation results comparison.....                    | 13   |
| Figure 2.7: Divided two parts a) transition (b) taper curve.....               | 14   |
| Figure 2.8: Radiation Pattern of the whole antenna a) Gain b) directivity..... | 15   |
| Figure 2.9: Impedance bandwidth of two antennas.....                           | 16   |
| Figure 3.1: Tapered curvature modeled as a stepline.....                       | 19   |
| Figure 3.2: Input reflection coefficient for an exponential taper.....         | 20   |
| Figure 3.3: Substrate with different dielectric constant.....                  | 21   |
| Figure 3.4: Substrate with different height.....                               | 22   |
| Figure 3.5: Opening rate R effects.....  | 24   |
| Figure 4.1: Different Sketches of Micro-strip / Slot-line Transition.....      | 26   |
| Figure 4.2: Microstrip to slotline transition .....                            | 27   |
| Figure 4.3: Reactance of the microstrip stub $X_m$ .....                       | 32   |
| Figure 4.4: Reactance of slotline cavity $X_s$ .....                           | 32   |

|  |    |
|--|----|
| Figure 4.5: Reactance X.....   | 32 |
| Figure 4.6: Reflection coefficient $S_{11}$ (microstrip stub is resonant at 4GHz) .....                          | 34 |
| Figure 4.7: Reflection coefficient $S_{11}$ (slotline cavity is resonant at 4GHz) .....                          | 34 |
| Figure 4.8: Fractional impedance bandwidth in regard to $D_s$ and $R_{rad}$ .....                                | 35 |
| Figure 5.1: Final antenna modeled by CST.....  | 39 |
| Figure 5.2: Simulated $S_{11}$ of the final design.....  | 41 |
| Figure 5.3: Simulated E field of the final design a) $f=4\text{GHz}$ b) $f=8\text{GHz}$ c) $f=12\text{GHz}$ .... | 42 |
| Figure 5.4: Simulated radiation pattern ( $f=8\text{GHz}$ ) of the optimal design.....                           | 43 |
| Figure 5.5: Radiation pattern: E plane at $f=4, 8, 12\text{ GHz}$ .....  | 44 |
| Figure 5.6: Radiation pattern: H plane at $f=4, 8, 12\text{ GHz}$ .....  | 44 |
| Figure 5.7: Simulated gain of the final design.....  | 45 |
| Figure 5.8: Excitation signal and its derivation.....  | 46 |
| Figure 5.9: Radiated impulse at main lobe direction (normalized) .....   | 46 |
| Figure 6.1: Fabricated antenna a) front view b) back view.....   | 47 |
| Figure 6.2: $S_{11}$ of the final design: Measured VS simulated .....  | 48 |
| Figure 6.3: Gain of the final design: Measured VS simulated .....  | 50 |
| Figure 6.4: Impulse response of the final design: Measured VS simulated .....                                    | 51 |

## CHAPTER I

### INTRODUCTION

#### **1.1 Background**

Ultra wideband (UWB) communications represent an emerging technology that attracts the attention of both industry and academia.<sup>[1]</sup> A UWB antenna, as the indispensable component of every communication system, is essential to high frequency communications and electronic systems for radiating or receiving electromagnetic (EM) energy.

The Vivaldi antenna as a typical UWB antenna, possessing high efficiency, wide bandwidth, light weight, small size, and simplicity, has been employed in various research and technological fields since it was introduced by Gibson in 1979<sup>[2]</sup>. The first studies were mostly experimental and researchers provided some empirical design formulas. In 1986, the simple case of a TSA without a substrate was first analyzed,<sup>[3]</sup> and later on more effective methods were gradually introduced.

Nowadays, the use of Vivaldi antennas ranges from commercial communication to radio astronomy.<sup>[4-7]</sup> The simple and inexpensive manufacturing of these antennas, due to the printed circuit technology, well matches their irradiative features, providing a very wide band of operations. The applications such as microwave imaging for near fielding

scanning<sup>[8]</sup>, are being employed as sensors in ground penetrating radar systems,<sup>[9,10]</sup> in recent high technology ultra wideband(UWB) designs.

## 1.2 Current research

Achieving a successful design is usually costly and time consuming since the relationship between antenna parameters and antenna performance are not well understood.

Studies have been performed to investigate the effect of the curvature. Experiments conducted by Lee and Simons<sup>[11]</sup> have showed that the curvature of tapered profile has a significant impact on the gain, beamwidth and bandwidth of TSAs. However, there is no more information about how the curvature impacts those performances. Sutinjo and Tung<sup>[12]</sup> did deeper research on the curvature of Vivaldi antenna and found the optimal opening rate of the curvature. However, the ‘optimal’ opening rate is only regarding to the VSWR instead of the overall performance. There are many claims<sup>[13,14]</sup> that the feed generally determines the high-frequency limit while the aperture size determines the low-frequency limit. But very few attempts have been made to justify this assertion in a rigorous manner.

How good can a Vivaldi antenna be? How much spaces left before the limitation is reached? Currently, there has been insufficient study of these questions. Although some researchers have been working on improving the performance of Vivaldi antenna and doing the optimization, their researches mainly focus on one aspect of the performances. Chao Deng and Yong-jun Xie<sup>[15]</sup> designed Vivaldi Antenna using Resistive Loading, which makes the impedance bandwidth 1~20GHz. However the Gain is quite low, between 0.9~7.8dB. Antipodal Vivaldi antenna designed by Alexander N. Sharp, Ross

Kyprianou<sup>[16]</sup> has gain bandwidth from 2~20GHz without considering the impedance and radiation pattern.

### **1.3 Objective**

In conclusion, the current research on Vivaldi antenna is insufficient in the following two aspects:

- Some assertions about how antenna parameters influence the antenna performances are not verified or experimentally verified.
- Only focus on one aspect of performance and do not conclude others when improving the antenna design.

The objective of my research aims at those deficiencies, investigating how the Vivaldi antenna parameters determine the performance and trying to design an optimal Vivaldi antenna which reaches the limitation taking overall performance into consideration.

### **1.4 Organization**

The thesis has been divided into a total of seven chapters.

Chapter 2 begins with an introduction of the basic Vivaldi antenna. The characteristics and design considerations will give an insight into the operations of the antenna. The method of approach of this paper is mainly introduced at the end of this chapter.

Chapter 3 provides an in depth look into the principles of the taper curve part of the Vivaldi antenna. The key parameters on the taper curve effect on the antenna performance are studied and the ways of improving the usable gain bandwidth are found.

Chapter4 focuses on the transition from the microstrip to slotline. After basic circuit model of the transition and the key parameters effect on the antenna performance are well studied, a novel method to design the key parameters on the transition part in order to get wider impedance bandwidth is proposed and also verified by CST simulation results.

Chapter 5 gives the optimal Vivaldi antenna design in detail by combining the methods of improving the impedance bandwidth and usable gain bandwidth concluded in Chapter 3 and Chapter4 .The important characteristic parameters are simulated by CST.

Chapter 6 provides the measurement results of the fabricated optimal Vivaldi antenna designed in Chapter5. The comparison between the simulation and measurement results are made.

Finally, the conclusion and contribution are made in Chapter 7.

## CHAPTER II

## VIVALDI ANTENNA

**2.1 Taper types of TSA**

There are many taper profiles for Tapered-Slot Antennas (TSA). The Vivaldi antenna is a special type of TSA with an exponential flare profile. Figure 2.1 shows different planar designs and we can observe that each antenna differs from the other only in the taper profile of the slot. Planar tapered slot antennas have two common features. The radiating slot acts as the ground plane for the antenna and the antenna is fed by a balanced slotline.

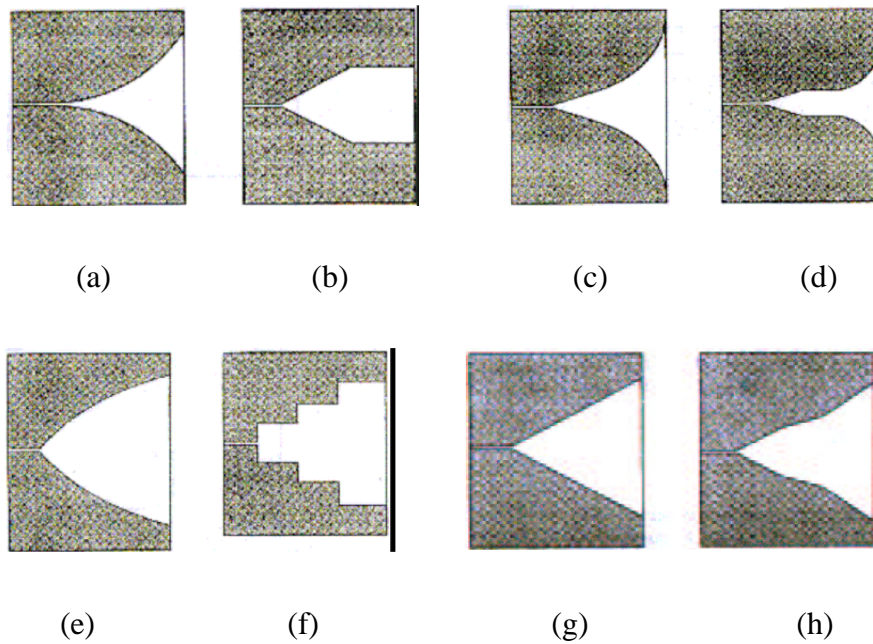


Figure 2-1 Different taper-styles of the TSA

(a) Exponential (Vivaldi); (b) Linear constant; (c) Tangential; (d) Exponential-constant; (e) Parabolic; (f) Step-constant; (g) Linear; (h) Broken-linear<sup>[14,17]</sup>

## 2.2 Principle of Vivaldi antenna

The Vivaldi antenna is the focus of this research work due to its performance in comparison to other kinds of TSAs including higher gain, wider bandwidth, and lower reflection.

From the view point of its appearance and physical characteristics, the Vivaldi is among the printed antennas. The TSA consists of a gradually widening slot in a metallic plate with or without a substrate and without a ground plane. For most efficient coupling, the narrow end of the slot is used for connecting to devices such as, the sources and mixing diodes. It belongs to the class of traveling wave antennas. The waves travel down the curved path of the flare along the antenna. In the region where the separation between the conductors is small when compared to the free-space wavelength, the waves are tightly bound and as the separation increases, the bond becomes progressively weaker and the waves get radiated away from the antenna.<sup>[2]</sup>

The tapered-slot antennas utilize a traveling wave propagating along the antenna structure because the phase velocity  $V_{ph}$  is less than the velocity of light in free space or  $V_{ph} < c$  (as well as the limiting case when  $V_{ph} = c$ )<sup>[18]</sup>. Therefore, they produce radiation in the endfire direction at the wider end of the slot in preference to other directions. The limiting case of  $V_{ph} = c$  relates to the case of the antenna with air as the dielectric and consequently the beamwidth and the sidelobe level are considerably greater than with a dielectric present. Also, the phase velocity and the guide wavelength vary with the

change in the thickness, dielectric constant and taper design. These antennas have symmetric radiation pattern with side lobes (see Figure 2.2).

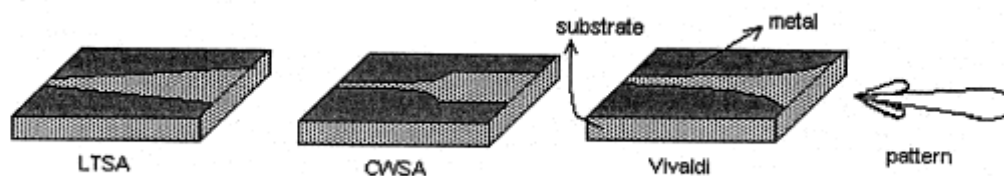


Figure 2.2 Typical radiation pattern of TSA<sup>[18]</sup>

At different frequencies, different parts of the antenna radiate, while the radiating part is constant in wavelength.<sup>[2]</sup> Thus the antenna theoretically has an infinite bandwidth of operation and can thus be termed frequency independent. As the wavelength varies, radiation occurs from a different section which is scaled in size in proportion to the wavelength and has the same relative shape. This translates into an antenna with very wide bandwidth. Again referring to Figure 2.3 it can be seen that the Vivaldi antenna is divided into two areas:

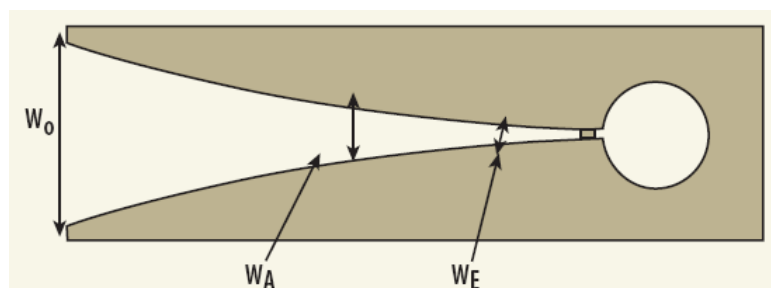


Figure 2.3 Vivaldi antenna taper structure

- a propagating region defined by  $W_E < W < W_A$
- a radiating region defined by  $W_A < W < W_0$

where  $W_E$  is the input slot width,  $W_A$  is the slot width at the radiating area, and  $W_O$  is the output slot width.

### 2.3 Feeding techniques

In order to couple microwave signals to the antenna from a planar microstrip circuit, a transition is needed. Many feed techniques are available, with the most common approaches being coaxial feed lines and microstrip feed lines.

A microstrip-to-slotline transition offers many advantages compared to other feed mechanisms. This transition can be easily fabricated by a conventional photo-etching process. In addition, two-sided printed-circuit boards (PCBs) can be fabricated with microstrip on one side and slotline on the other to achieve a compact transition. It consists of a slot, etched on one side of the substrate, crossing an open circuited microstrip line, located on the opposite side, at a right angle. The slot extends to one quarter of a wavelength ( $\lambda_s$ ) beyond the microstrip and the microstrip extends one quarter of a wavelength ( $\lambda_m$ ) beyond the slot<sup>[19]</sup> as shown in Figure 2.4. A more detailed description of the transition and the design procedure is given in Chapter 4.

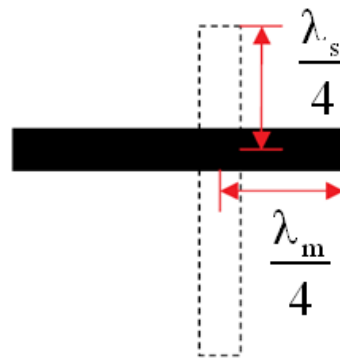


Figure 2.4 Microstrip to slotline transition

As discussed earlier, a proper feed structure design becomes essential to maximize the bandwidth.

Theoretically, the Vivaldi antenna is capable of having an infinite operating bandwidth, while practically the operating bandwidth is limited by the finite dimensions of the antenna and by the transition from the feeding transmission line to the slot line of the antenna<sup>[14]</sup>. The feed generally determines the high-frequency limit while the aperture size determines the low-frequency limit<sup>[13]</sup>. These claims have not been explained and verified sufficiently. However, we can get a general concept that to achieve a wider bandwidth, it is imperative for the designer to have in mind the following two aspects:

- Transition from the main input transmission line to the slot line for the antenna feeding. This is designed for a low reflection coefficient to match the potential of the antenna.
- The dimensions and shape of the antenna, to obtain the required beam width, sidelobes and back lobes over the operating range of frequencies.

## **2.4 Method of approach**

From above study and discussion, we get a general idea of the Vivaldi antenna's construction, operating principles, feeding techniques. It is necessary to figure out what are the factors limiting the antenna bandwidth before attempting to design an improved Vivaldi antenna. Moreover, the antenna will be improved not only regarding to either reflection coefficient or gain but both of them. The methods of approach for this research lie on following three aspects.

### 2.4.1 Multi-objective

A UWB antenna is distinguished by its large bandwidth. Thus, considering bandwidth is an appropriate place to make an examination of a UWB antenna's properties<sup>[33]</sup>. There are various ways to express bandwidth, including fractional or percent bandwidth. The ways in which bandwidth can be defined include impedance, pattern, gain, and radiated bandwidths.

One approach uses the impedance bandwidth of an antenna. Consider a particular impedance goal such as  $-10\text{dB } S_{11}$ . The upper and lower operating frequencies are defined as the endpoints of the frequency range across which antenna meets or exceeds the impedance goal.

An alternate method for defining antenna bandwidth utilizes the gain bandwidth of an antenna. For a constant gain antenna, the upper and lower operating frequencies may be taken as those points where the gain falls  $-3\text{dB}$  or  $-10\text{dB}$  below the in-band constant gain<sup>[33]</sup>. This approach also suffers from some problems. The gain of many antennas increases as a function of frequency. For instance, the gain of a constant aperture antenna varies as  $f^2$ . Thus, gain increases  $6\text{dB}$  per octave. A two-octave antenna experiences  $12\text{dB}$  increase in gain across its operating band. An arbitrary fixed gain cutoff becomes difficult to justify for such antenna.

Still another method employs pattern bandwidth. With this approach, the upper and lower frequencies are those between which an antenna's pattern meets a particular specification. For instance, one may desire an omnidirectional antenna in the azimuthal plane. The ends of the antenna's operating bandwidth may be taken as those frequencies

where gain varies by more than 3dB in the azimuthal plane. Here again, this may not accurately reflect changes in other parameters, such as matching, that may render the antenna unsuitable for use.

A holistic approach that takes into account all of the properties of an antenna important to a particular application is the preferred way to describe antenna bandwidth. In practice, an UWB system will place demands on an antenna for matching, gain, radiation pattern, spectral response, and other properties.

Here we define a usable gain which combines the properties of gain and radiation pattern. It means the gain is bigger than 3dBi and the main lobe of the radiation pattern has no break up of the main lobe. Consequently, we consider the impedance bandwidth, usable gain bandwidth are the most significant properties of a Vivaldi antenna. Therefore, we apply the two types of bandwidth as the indicators to represent the performance of Vivaldi antenna in the following work.

Table2-1: Bandwidth indicators and related quantitative standards

| <b>Bandwidth indicators</b> | <b>quantitative standard</b>                                 |
|-----------------------------|--|
| Impedance bandwidth         | $S_{11} \leq -10\text{dB}$                                   |
| Usable gain bandwidth       | gain $\geq 3\text{dBi}$ & radiation pattern without break up |

#### **2.4.2 Multiple simulation tools**

Both HFSS and CST simulation tools we used to verify the reliability of whole antenna design.

HFSS is the industry-standard simulation tool for 3D full-wave electromagnetic field simulation.<sup>[37]</sup> It utilizes Finite Element Method (FEM) to compute the electrical

behavior of high-frequency and high-speed components. As a successful engineering design tool, HFSS can process the solution automatically where users are only required to specify the geometry, material properties and desired output.

HFSS provides E- and H-fields, currents, S-parameters and near and far radiated field results. From here HFSS will automatically generate an appropriate, efficient and accurate mesh for solving the problem using the proven finite element method. Users rely on the accuracy, capacity, and performance of HFSS to design high-speed components including on-chip embedded passives, IC packages, PCB interconnects, and high-frequency components such as antennas, RF/microwave components, and biomedical devices.

CST MICROWAVE STUDIO® (CST MWS) is a specialist tool for the fast and accurate 3D EM simulation of high frequency problems. It offers a broad range of solver technology in both time and frequency domain. It employs Finite Integration Technique and enables the fast and accurate analysis of high frequency (HF) devices such as antennas, filters, couplers, planar and multi-layer structures and SI and EMC effects.<sup>[38]</sup> Besides user friendly, CST MWS provides users an insight into the EM behavior of your high frequency designs.

Users are given great flexibility when dealing with a wide application range through the variety of available solver technologies. Besides the flagship module, the broadly applicable Time Domain solver and the Frequency Domain solver, CST MWS offers further solver modules for specific applications. Filters for the import of specific CAD files and the extraction of SPICE parameters enhance design possibilities and save time.

In addition, CST MWS is embedded in abundant industry standard workflows through the CST design environment.

Since FEM is a frequency domain method which is used by HFSS while CST MWS provides both Frequency Domain solver and Time Domain solver, CST MWS has advantages for electromagnetic wideband problems.

As a comparison, both HFSS and CST tools we used to simulate for Vivaldi antenna with exactly the same configuration as follows: RO3003 board with  $\epsilon_r = 3$ ,  $h = 0.8\text{mm}$ ,  $L = 230\text{mm}$ ,  $W = 120\text{mm}$ , opening rate  $R = 0.015\text{mm}^{-1}$ ,  $D_s = 14.2\text{mm}$ ,  $R_{rad} = 12\text{mm}$ .

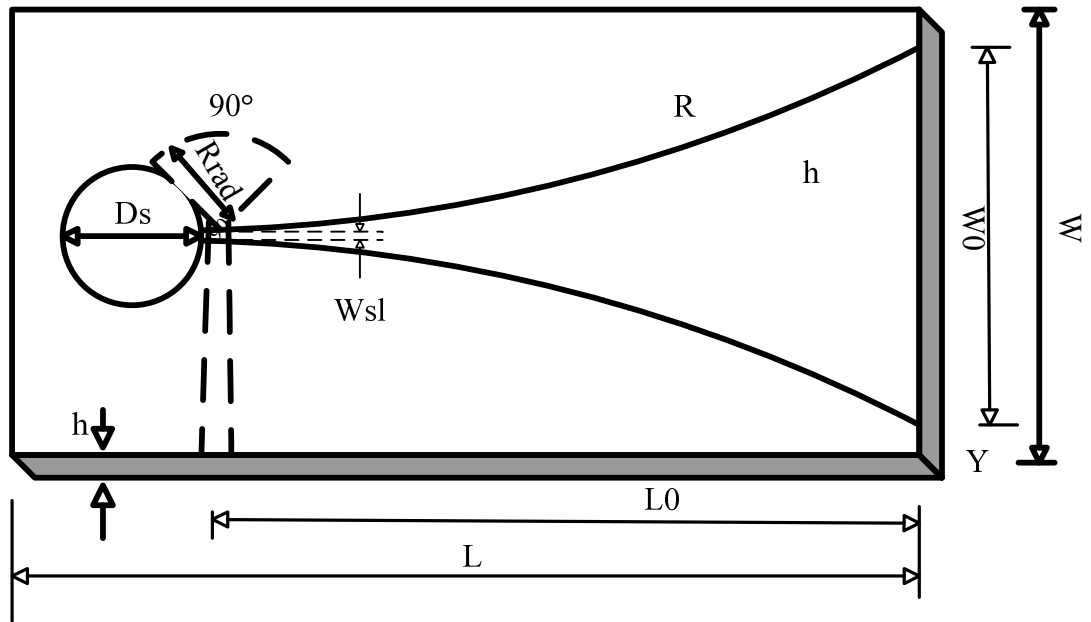


Figure 2.5 Vivaldi antenna configuration

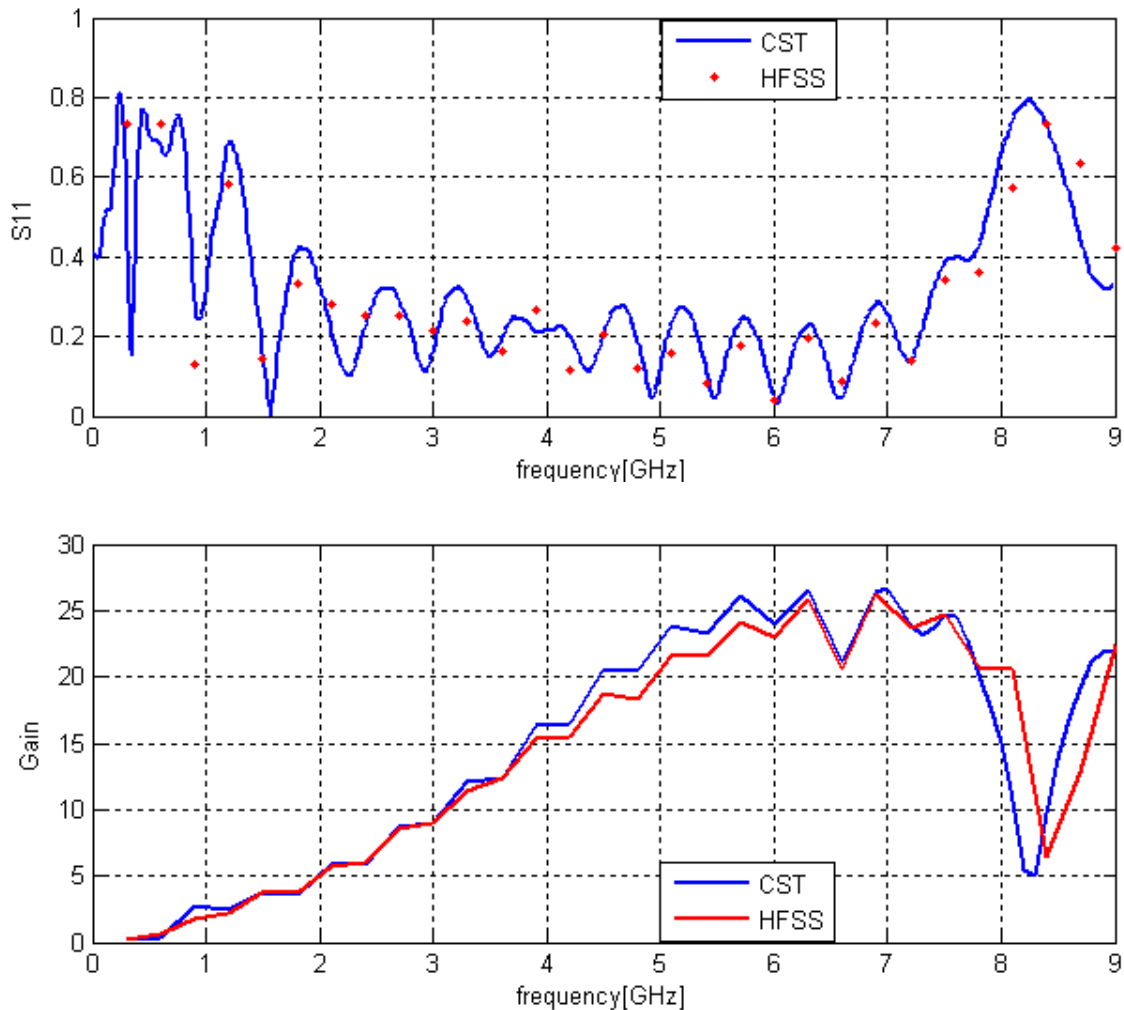


Figure 2.6 CST and HFSS simulation results comparison a) S11 b) Gain (not in dB)

From the simulation results, which are shown in Figure 2.6, we can see that both reflection coefficients achieved by HFSS and CST are quite closed to each other, and the gains have the same pattern. It gives confidence that we will get the similar experimental results of the physical antenna which is fabricated using the dimensions of the simulation model.

It is noted that HFSS consumes 32h04m22s for the whole simulation, while CST simulation only consumes 1h, 0m 39s, which shows CST has significant advantage regarding the simulation time.

### 2.4.3 Division into two parts

We divide the whole Vivaldi antenna into two parts: taper curve part and transition from microstrip to slotline, as it is shown in Figure 2.7.

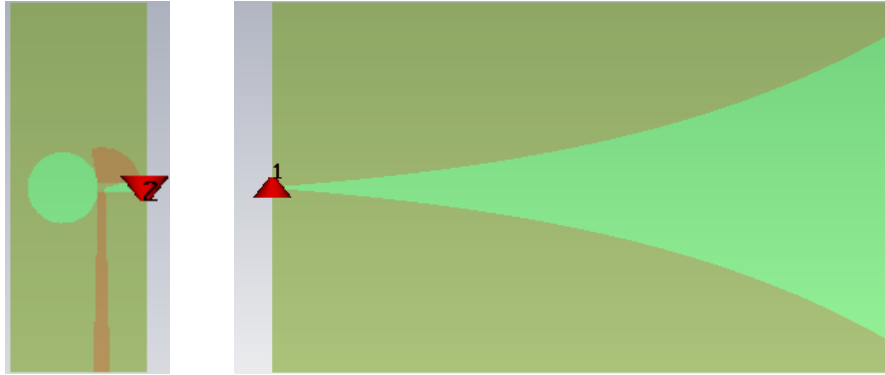


Figure 2.7 Divided two parts a) transition (b) taper curve

This idea was inspired by the current research results, such as “the feed generally determines the high-frequency limit”. which indicates that some properties of the antenna are totally determined by some specific part or certain parameter of the structure.

It greatly reduces the simulation time compared to doing a whole antenna simulation. In the previous simulation, as we mentioned, CST consumes 1hour,0m 39s for the whole antenna simulation. After implementing the 2 parts division, the transition part costs 2m,3s and the taper curve part costs 27 m, 23 s which saves more than 50% simulation time.

Moreover, it will be easier for us to find those relationships in order to find the potential methods to improve the performance of the antenna.

There are two antennas models (Antenna 1 and Antenna 2) having the same substrate and taper configuration as follows: Rogers RO3003 (lossy)  $\epsilon_r = 3.0$   $h=1.27\text{mm}$ ,  $R=0.02\text{mm}^{-1}$ ,  $D_s=14.2\text{mm}$ ,  $R_{rad}=10\text{mm}$ ,  $W_{m1}=1\text{mm}$ ,  $W_{m2}=3.25\text{mm}$ . The only

difference is the transition part configuration. For Antenna#1,  $D_s=14.2\text{mm}$ ,  $R_{rad}=10$ , and for Antenna#2,  $D_s=14.2\text{mm}$ ,  $R_{rad}=18\text{mm}$ .

From Figure 2.8, we can see that directivity of the whole antenna dominantly depends on the taper curve part. As we know that  $Gain = Directivity \times Efficiency$ , therefore the transition part only affects the transmission efficiency.

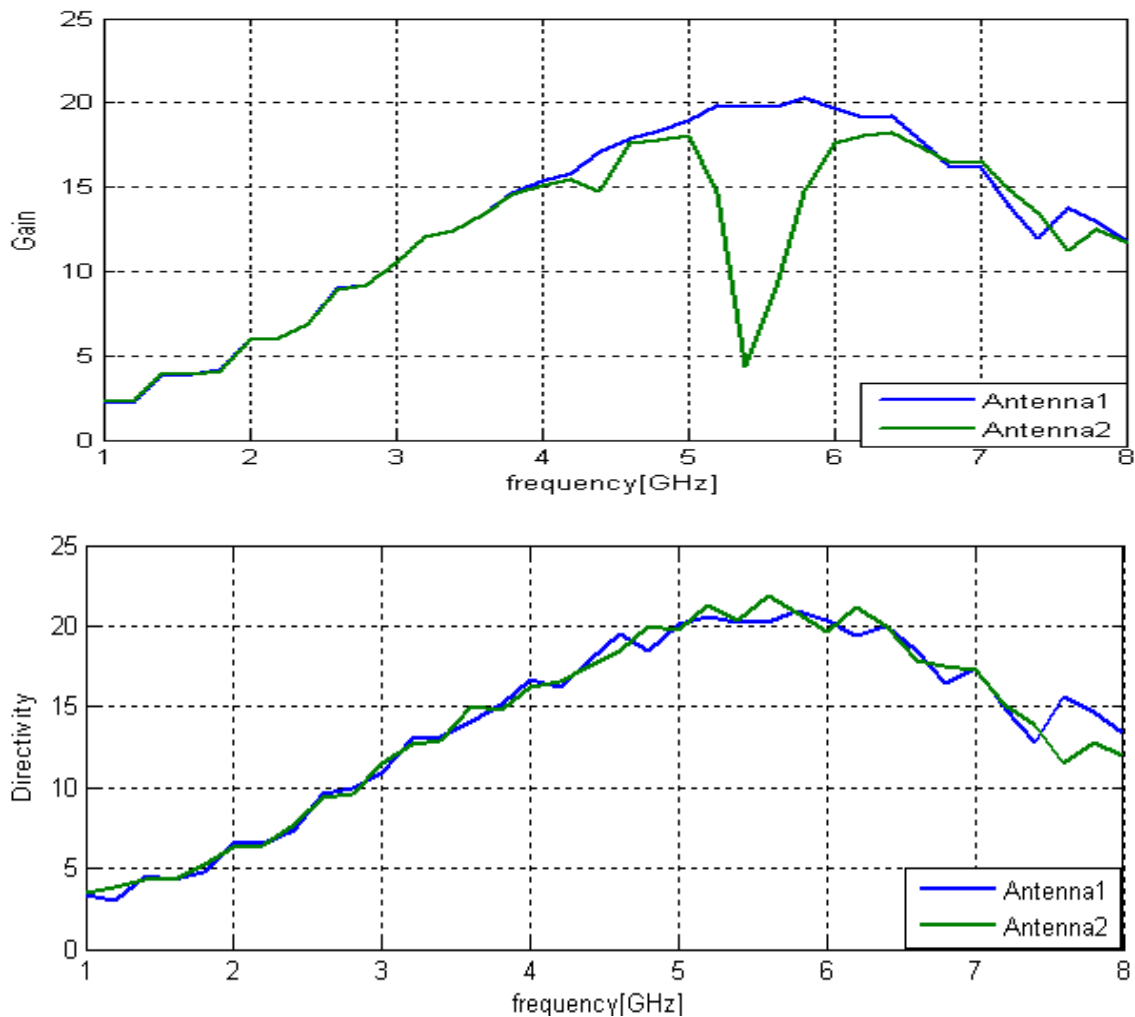


Figure 2.8 Radiation Pattern of the whole antenna  
 a) Gain (not in dB) b) Directivity

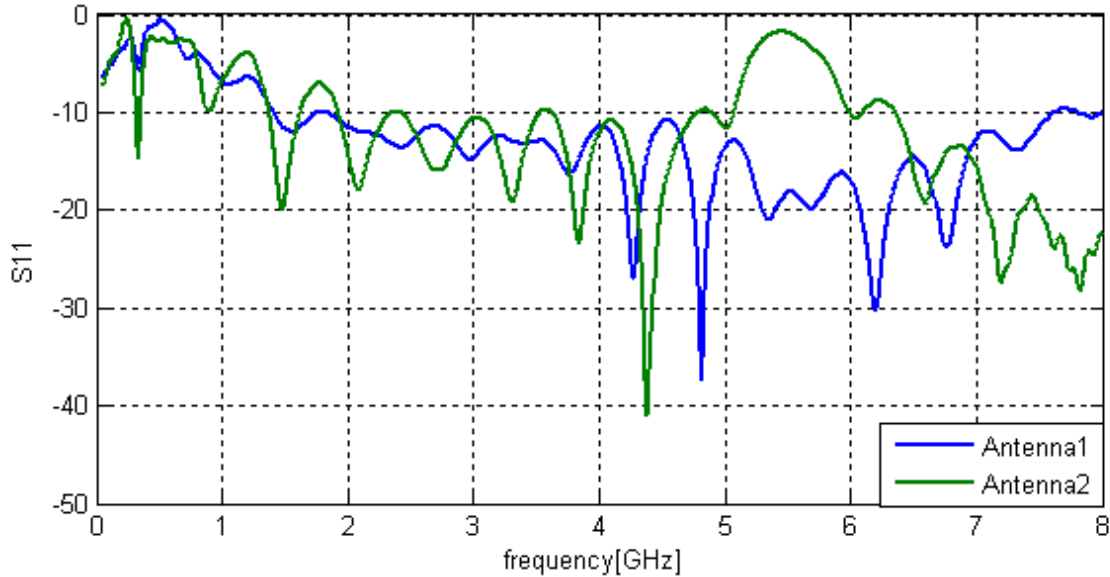


Figure 2.9 Impedance bandwidth of two antennas

It is noticeable that the transition configuration difference of Antenna1 and Antenna2 is only a different microstrip radial stub length. From Figure 2.8b, we already see the  $R_{rad}$  affects the transmission efficiency. In Figure 2.9, we can see that the higher cutoff frequencies of the two antennas are totally different.

With regard to the impedance bandwidth of the whole antenna, the taper curve has no limitation on the higher cutoff frequency. This is determined by transition part. To be more accurate, it is totally determined by the microstrip radial stub length. The length of the taper curve limits the lower cutoff frequency. At the same time, parameters on transition part also affect the lower frequency range. A more detailed description will be discussed in Chapter 3 and Chapter 4.

Of course, the disadvantage also comes out. It is noted that besides the port at the end of the transition, there are two more ports, Port1 and Port2, which are caused by the separation (see red arrow in Figure 2.7). We regard the taper curve part as load and terminate the two ports using the loads at the same constant value, while to be accurate

the input impedance of the taper curve is supposed to vary with frequency. The good thing is the input impedance is close to a constant value at higher frequencies. Therefore, the error will be noticeable only at low frequency region.

## CHAPTER III

### RESEARCH ON TAPER PROFILE

As we mentioned in Chapter2, the whole antenna is separated into two parts. In this chapter, we focus on the taper curve part to see how the parameters on taper curve part affect the performance regarding to both impedance bandwidth and usable gain bandwidth. All the conclusions are made based on CST simulation results before they are verified by measurement.

#### 3.1 Exponential taper

##### 3.1.1 Taper stepline model

The taper curve part of the Vivaldi antenna of total length  $L$  is modeled as a stepline having  $N$  slot sections having a different width  $W_n$  and length  $L_n$  as shown in Figure 3.1.

We are familiar with the Quarter-wave Transformer. To implement a Quarter-wave match between two transmission lines with impedances  $Z_1$  and  $Z_2$  is to use a matching section whose impedance  $Z$  is the geometric average of the two line impedances:

$$Z = \sqrt{Z_1 Z_2} \quad (3-1)$$

In a multi-section Quarter-wave transformer used to match two transmission lines with different characteristic impedances, the change in impedance level is obtained in a number of discrete steps.

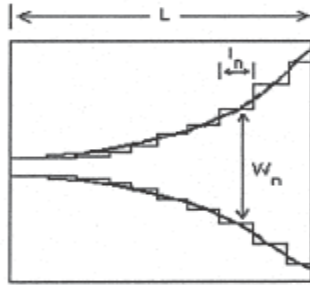


Figure 3.1 Tapered curvature modeled as a stepline

### 3.1.2 Tapered transmission line

An alternative is to use a tapered transition which has characteristic impedance that varies continuously in a smooth fashion from the impedance of one line to that of the other line.<sup>[20]</sup> A transition of this type is referred to as a tapered transmission line.

Tapered transmission line has normalized impedance  $\bar{Z}$  which is a function of a distance  $x$  along the taper. There is an approximation to the continuous taper by considering it to be made up of a number of sections of line of differential length  $dx$ . It is assumed that the total reflection coefficient can be computed by summing up all the individual contributions, the input reflection coefficient is given by

$$\Gamma_i = \frac{1}{2} \int_0^L e^{-2j\beta x} \frac{d}{dx} (\ln \bar{Z}) dx \quad (3-2)$$

The Vivaldi antenna is one of the TSAs with exponential taper profile. Exponential taper is one for which  $\ln \bar{Z}_L$  varies linearly, and hence  $\bar{Z}$  varies exponentially, from 1 to  $\ln \bar{Z}_L$ ; that is ,

$$\ln \bar{Z} = \frac{x}{L} \ln \bar{Z}_L \Rightarrow \bar{Z} = e^{(x/L) \ln \bar{Z}_L} \quad (3-3)$$

Substituting (3-3) into (3-2) gives

$$\Gamma_i = \frac{1}{2} \int_0^L \frac{\ln \bar{Z}_L}{L} e^{-2j\beta x} dx = \frac{1}{2} \ln \bar{Z}_L e^{-2j\beta L} \frac{\sin(\beta L)}{\beta L} \quad (3-4)$$

A plot of  $|\Gamma_i|$  versus  $\beta L$  is given in Figure 3.2. For a fixed length of taper, this is a plot of  $|\Gamma_i|$  as a function of frequency. Note that when  $L$  is great than  $\lambda/2$ , the reflection coefficient is quite small, the first minor lobe being about 22% of the major lobe maximum.

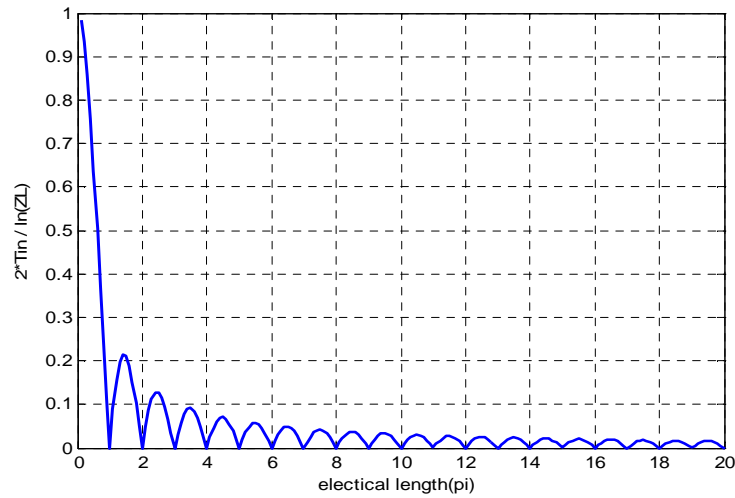


Figure 3.2 Input reflection coefficient for an exponential taper

## 3.2 Parameter effect

### 3.2.1 Substrate size

Basically, for a radiation traveling mode, the value for taper length should exceed the wavelength of free space at the lower frequency range<sup>[21]</sup> and the width should be greater than the half the wave-length of free space<sup>[22]</sup>. So

$$\begin{cases} L > \lambda \\ W > \lambda/2 \end{cases} \quad (3-5)$$

where  $\lambda$  is the free space wavelength at the lowest frequency.

Theoretically a longer board makes small value of reflection coefficient at lower frequency which also indicates in Figure 3.2. In other word, the length  $L$  gets longer, the lower cutoff frequency gets lower, which shows the potential to obtain wider impedance bandwidth.

This statement is in agreement with the one claim that the operating bandwidth is limited by the finite dimensions of the antenna<sup>[14]</sup>.

### 3.2.2 Substrate dielectric constant

A substrate with lower dielectric constant  $\epsilon_r$  can prevent the radiation pattern from breaking up at higher frequency, which increases the usable gain bandwidth significantly. This conclusion is in accordance to Figure 3a and 4a of reference [23]. At the same time, the reflection coefficient  $S_{11}$  gets lower among the frequency range.

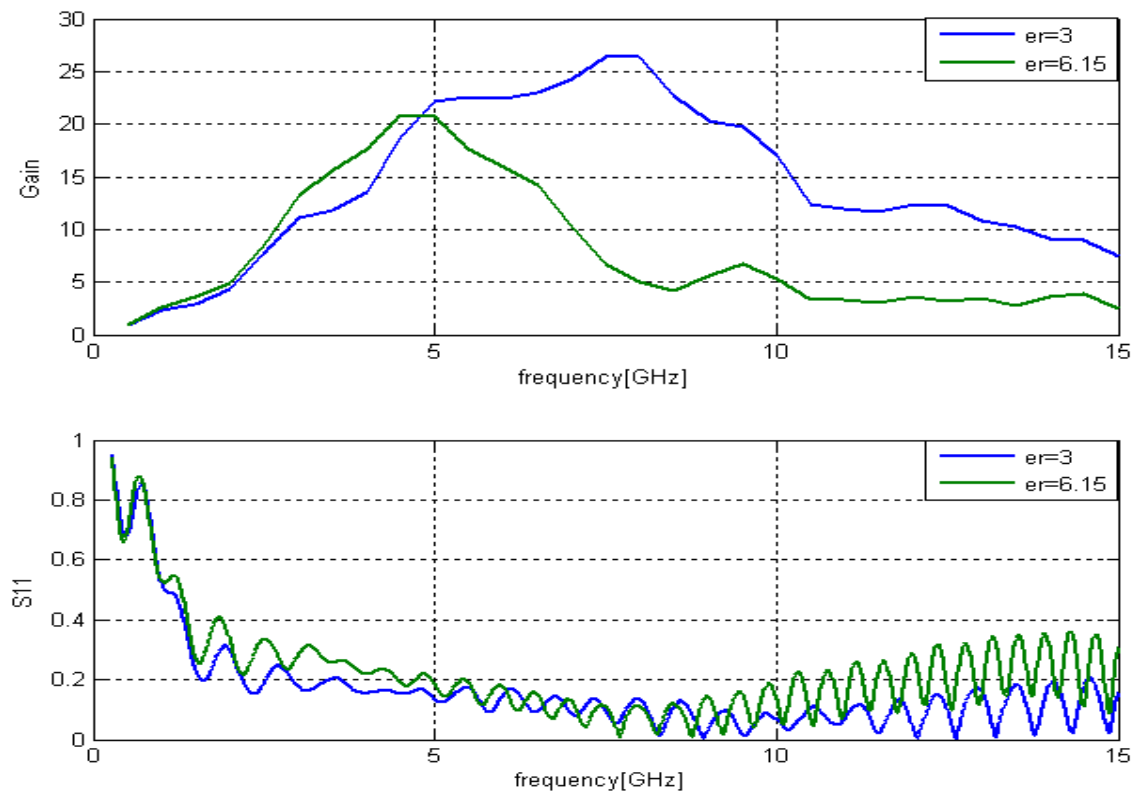


Figure 3.3 Substrate with different dielectric constant

a) Gain (not in dB)    b)  $S_{11}$

### 3.2.3 Substrate thickness

Substrate with thinner height  $h$  can prevent the radiation pattern from breaking up at higher frequency, which increases the usable gain bandwidth significantly. At the same time, the reflection coefficient  $S_{11}$  gets lower among the frequency range, which shows agreement with Figure 6.b of the reference [24].

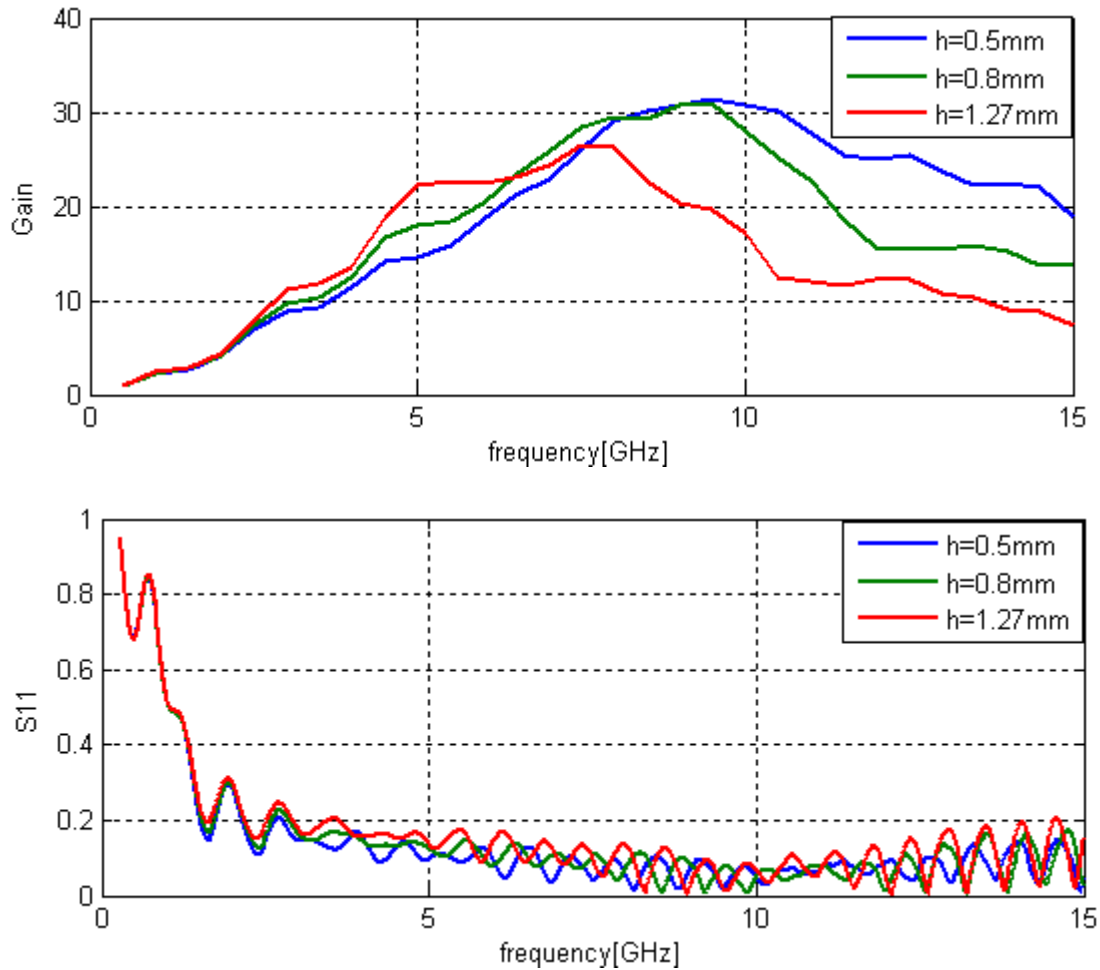


Figure 3.4 Substrate with different height a) Gain (not in dB) b) S11

### 3.2.4 Curvature profile

As we mentioned in Section 3.1.2, in the exponential taper,

$$\bar{Z} = e^{(x/L)\ln\bar{Z}_L} \quad (3-6)$$

The slotline portion is modeled by N steps. The characteristic impedance at each stepline can be calculated by (3-6). To get smooth taper, we employ exponential to do the curve fit.

The exponential taper profile is defined by

$$y = C_1 e^{Rx} + C_2 \quad (3-7)$$

where  $C_1$  and  $C_2$  are the constants,  $R$  is the opening rate. If we suppose the two points  $P_1(x_1, y_1)$  and  $P_2(x_2, y_2)$  as the beginning and the end points, then

$$\begin{aligned} C_1 &= \frac{y_2 - y_1}{e^{Rx_2} - e^{Rx_1}} \\ C_2 &= \frac{y_1 e^{Rx_2} - y_2 e^{Rx_1}}{e^{Rx_2} - e^{Rx_1}} \end{aligned} \quad (3-8)$$

The Vivaldi antenna is approximately frequency independent, at every wavelength a portion of the antenna radiates and when the wave length varies, this section changes which is scaled in size in proportion to the wave length<sup>[25]</sup>.

The taper curvature profile plays an important role in overall performance. However, those analyses are made only concerning reflection coefficient. When we consider overall performance of the taper and the whole Vivaldi antenna, radiation pattern should be considered first. However, what is size of taper affection on the gain of the taper? What is the relationship between the gain of the taper and the gain of whole antenna? Those questions are not well understood. This section attempts to determine this information.

The configuration is as follows: A Rogers RO3006 substrate with  $\epsilon_r = 6.15$  and thickness  $h=1.27\text{mm}$ ,  $L=200\text{mm}$ ,  $W=120\text{mm}$ ,  $Wl=100\text{mm}$ . The initial slot width is

$Wsl=0.5\text{mm}$ . The effect of  $R$  on the tapered slot VSWR and Gain are shown in Figure 3.6 respectively.

As the Figure 3.5 indicates, the opening rate  $R$  affects Both impedance match and Gain obviously: higher  $R$  has the tendency to make the radiation pattern split up from lower frequency and make the VSWR lower overall frequency range.

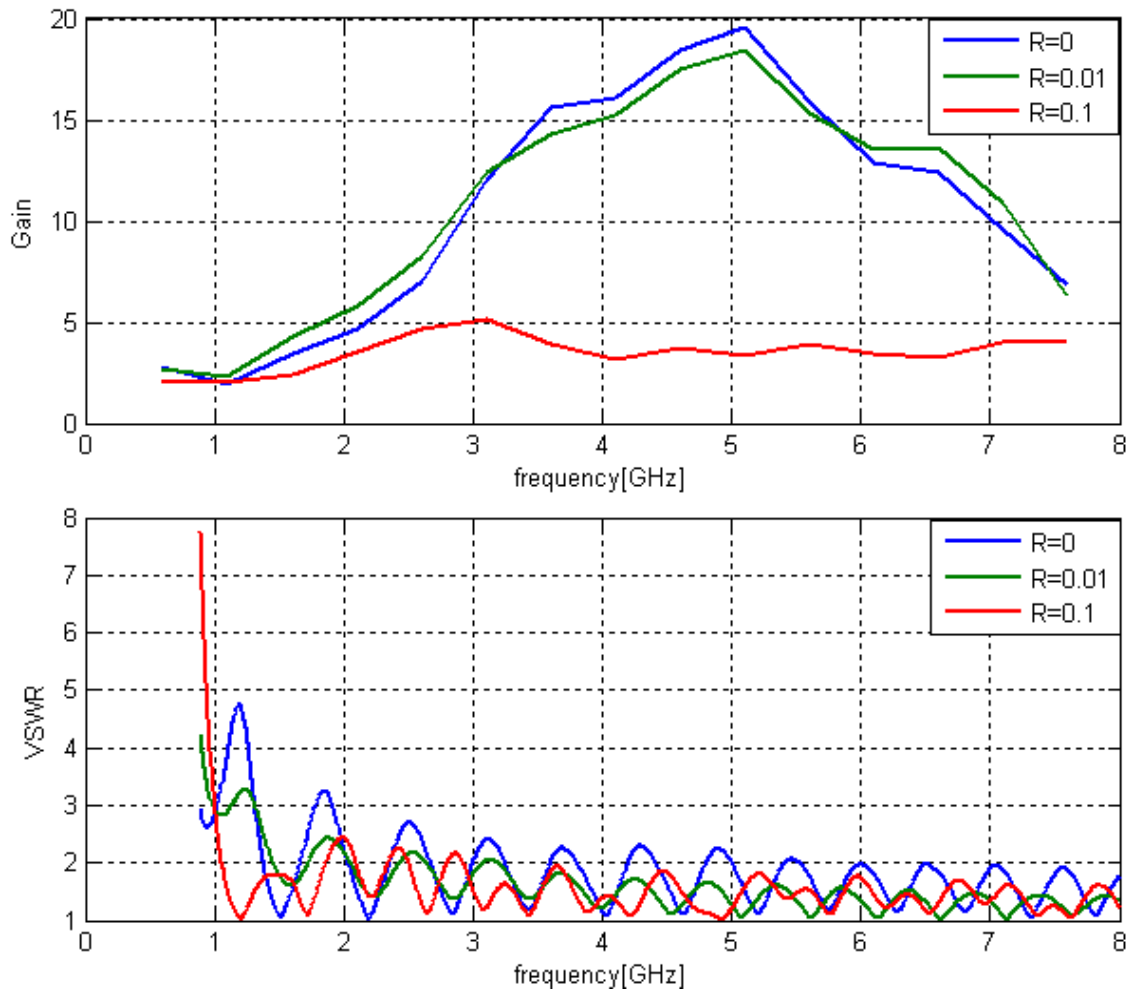


Figure 3.5 Opening rate  $R$  effects on a) Gain (not in dB) b) VSWR

### 3.3 Conclusion

In order to get wider usable gain bandwidth, it is recommended to use the substrate with lower dielectric constant and thinner thickness. A lower opening rate of the tapered curve can also increase the usable gain bandwidth, however, it decreases the impedance

bandwidth. Therefore, it is necessary to choose a proper opening rate by making tradeoff between two bandwidths.

Over all, an exponential tapered curve only affects the lower cutoff frequency. Therefore, if we wish to broaden the whole antenna's impedance bandwidth, especially for the high frequency range, transition from microstrip to slotline becomes the object to focus on.

## CHAPTER IV

## RESEARCH ON TRANSITION PART

**4.1 Transition types**

Schuppert<sup>[19]</sup> analyzed microstrip to slotline transition using transmission lines. His work included first four different sketches as given in Figure 4.1. He modeled the sketches as simple circuit models and showed that improved bandwidth is resulted in (b) than (a) by reactance compensation effect. He found out the circular shape provides also an improved flatness and the impedance bandwidth is better wider in (d) than (c).

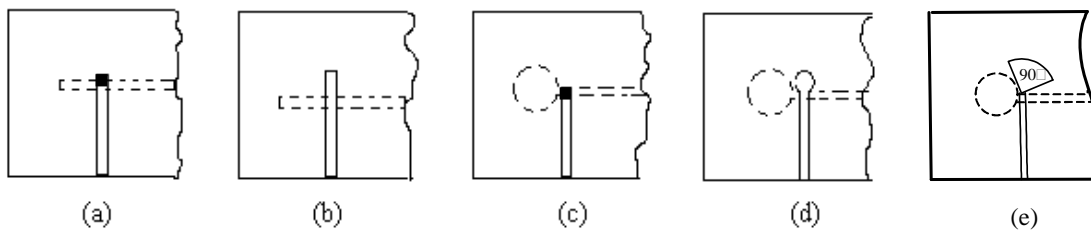


Figure 4.1 Different Sketches of Micro-strip (solid line) / Slot-line (dashed line) Transition

a) soldered microstrip short and (b) virtual short with uniform open microstrip and slotline (c) soldered microstrip short and circular slotline open circuit (d) nonuniform circular microstrip and slotline open circuit<sup>[19]</sup> (e) nonuniform radial microstrip and circular slotline open circuit

It is noted that the sketch in (d) suffers the problem of overlapping the line shapes between the microstrip and slotline cavity. Such overlapping generally disturbs the effectiveness of the microstrip ground plane. Currently, the radial microstrip stub instead

of a circular one is usually used since the geometry of the alleviate overlapping, as is shown in (e).

### 4.2 Equivalent circuit

The transition from the microstrip to slotline utilized in this paper is the sketch in (e). To have a better understanding of the sketch, we study the sketch in (b) with uniform straight stubs since it is the original structure of the sketch in (e) with nonuniform circular and radial stubs. The slotline, which is etched on one side of the substrate, is crossed at right angle by a microstrip conductor on the opposite side. The microstrip extends the length  $l_m$  beyond the slotline and the slotline extends with the length of  $l_s$  beyond the microstrip. The equivalent circuit of the above transition proposed by Chambers et al.<sup>[26]</sup> with the input on the microstrip line is shown in Figure 4.2(b).

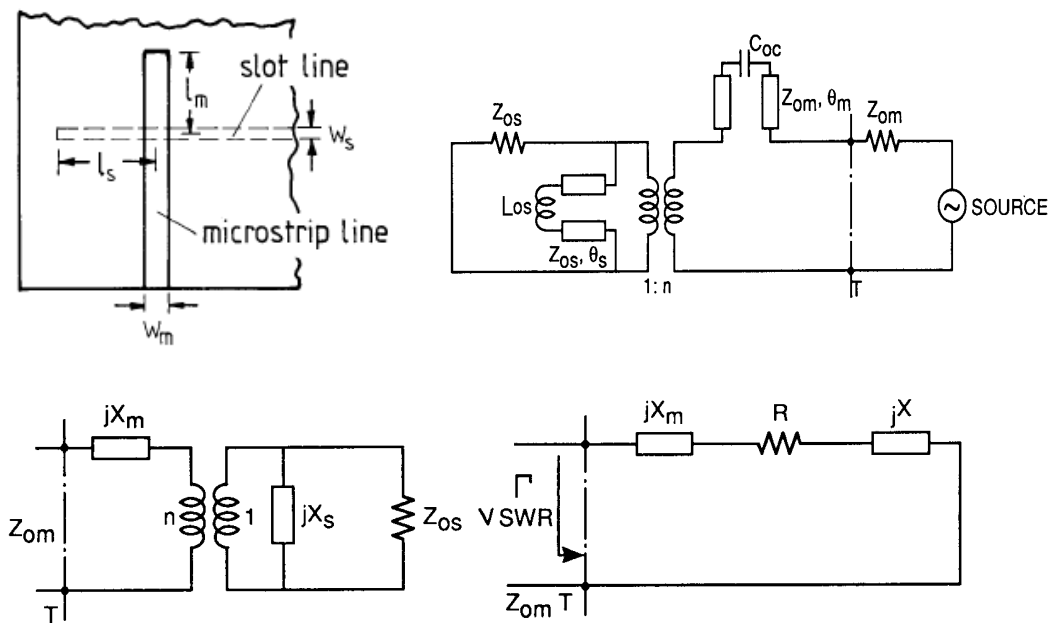


Figure 4.2 (a)Microstrip –to-slotline transition (b)transmission line equivalent circuit of a (c) reduced equivalent circuit of b (d) transformed equivalent circuit of (c)<sup>[26]</sup>

For further analysis the equivalent circuit in Figure 4.2(b) may be redrawn as in Figure 4.2(c).Here,

$$\begin{aligned}
jX_s &= Z_{0s} \frac{j\omega L_{0s} + jZ_{0s} \tan \theta_s}{Z_{0s} - \omega L_{0s} \tan \theta_s} \\
jX_m &= Z_{0m} \frac{1/j\omega C_{0c} + jZ_{0m} \tan \theta_m}{Z_{0m} + \tan \theta_m / \omega C_{0c}}
\end{aligned} \tag{4-1}$$

After transformation to the microstrip side, the equivalent circuit of Figure 4.2(c) reduces to that shown in Figure 4.2(d). In this circuit,

$$\begin{aligned}
R &= n^2 \frac{Z_{0s} X_s^2}{Z_{0s}^2 + X_s^2} \\
X &= n^2 \frac{Z_{0s} X_s}{Z_{0s}^2 + X_s^2}
\end{aligned} \tag{4-2}$$

Finally, the reflection coefficient is given by

$$\Gamma = \frac{R - Z_{0m} + j(X_m + X)}{R + Z_{0m} + j(X_m + X)} \tag{4-3}$$

Where,  $L_{0s}$  is the inductance of the shorted slotline;

$C_{0c}$  is the capacitance of the open microstrip;

$Z_{0s}$  is the slotline characteristic impedance;

$Z_{0m}$  is the microstrip characteristic impedance;

$\theta_s$  is the electrical length of the extended portion of slotline;

$\theta_m$  is the electrical length of the extended portion of microstrip;

$n$  is the transformer turns ratio, representing the magnitude of coupling between the microstrip and slotline.

In the approximate analysis reported by Knorr<sup>[26]</sup>, the transformer turns ratio  $n$  is determined from the knowledge of the slotline field components as

$$n = \frac{V(h)}{V_0} \tag{4-4}$$

where

$$V(h) = \int_{-b/2}^{b/2} E_y(h) dy \quad (4-5)$$

$V_0$  is the voltage across the slot ;  $E_y(h)$  is the electric field of slotline.

And  $E_y(h)$  may be written as

$$E_y(h) = -\frac{V_0}{b} \left\{ \cos \frac{2\pi u}{\lambda_0} h - \cot q_0 \sin \frac{2\pi u}{\lambda_0} h \right\} \quad (4-6)$$

Where,

$$q_0 = \frac{2\pi u}{\lambda_0} h + \tan^{-1} \left( \frac{u}{v} \right) \quad (4-7)$$

$$u = \left[ \epsilon_r - \left( \frac{\lambda_0}{\lambda_s} \right)^2 \right]^{1/2} \quad v = \left[ \left( \frac{\lambda_0}{\lambda_s} \right)^2 - 1 \right]^{1/2}$$

Substituting (4-6) and (4-7) into (4-4), the transformer turns ratio can be computed by

$$n = \cos \frac{2\pi u}{\lambda_0} h - \cot q_0 \sin \frac{2\pi u}{\lambda_0} h \quad (4-8)$$

Where,  $\lambda_0$  is the free space wavelength corresponding to center frequency  $f_0$  ;

$\lambda_s$  is the wavelength in slotline at center frequency  $f_0$  ;

$\lambda_m$  is the wavelength in microstrip at center frequency  $f_0$ .

### 4.3 Traditional parameter design

Impedance bandwidth limitation of cross-junction transition results mainly from the frequency dependence of  $X$  and  $X_m$ . Perfect impedance match between the microstrip to slotline can be achieved if

$$X = X_m = 0 \quad (4-9)$$

$$Z_{0m} = n^2 Z_{0s}$$

Then, the extended length  $l_s$  and  $l_m$  can be computed by transmission line theory

$$\begin{aligned} X = 0 \Rightarrow X_s = 0 \Rightarrow Z_{0s} - \omega L_{sc} \tan \theta_s = 0 \Rightarrow l_s &= \frac{\lambda_s}{2\pi} \tan^{-1} \left( \frac{Z_{0s}}{2\pi f_0 L_{sc}} \right) \\ X_m = 0 \Rightarrow 1/j\omega C_{0c} + jZ_{0m} \tan \theta_m = 0 \Rightarrow l_m &= \frac{\lambda_m}{2\pi} \tan^{-1} \left( \frac{1}{2\pi f_0 Z_{0m} C_{0c}} \right) \end{aligned} \quad (4-10)$$

Referring to the center frequency  $f_0$ , the extended microstrip section should appear as a short circuit and the extended slotline section should appear as an open circuit at the crossing reference plane. So the length of the two extended straight sections can be computed as

$$\begin{aligned} L_{sc} = 0 \Rightarrow l_s &= \frac{\lambda_s}{4} \\ C_{0c} = 0 \Rightarrow l_m &= \frac{\lambda_m}{4} \end{aligned} \quad (4-11)$$

Looking back to the sketch in (e), it is noticed that there is no accurate circuit model available for the nonuniform stubs calculating the inductance presented by the radial microstrip stub and the capacitance presented by the circular slotline cavity, although some efforts and progress have been made, for example Jerzy Chramiec<sup>[29]</sup> used resonant techniques to measure the reactance  $X_s$  of circular slotline cavity, and Vinding<sup>[28]</sup> proposed a formula of the reactance  $X_m$  based on an assumed radial-wave solution in the substrate dielectric with magnetic walls at the boundary of the stub, but accurateness has not been verified yet.

Most researchers regard the physical length of nonuniform stub (radius of the radial stub  $R_{rad}$  or the diameter of circular slotline cavity  $D_s$ ) can be approximately the length of a uniform straight stub. Therefore,

$$D_s = \frac{\lambda_s}{4}$$

$$Rrad = \frac{\lambda_m}{4}$$
(4-12)

In this way, both the radial stub and the slotline cavity are resonant at center frequency simultaneously if we regard the two stubs as resonators.

#### 4.4 Novel parameter design

As presented, to design a broad-band transition, traditionally, one attempts to realize slotline and microstrip resonators both resonant at center frequency  $f_0$ . However, it only guarantees the lowest  $S_{11}$  at one frequency point  $f_0$  and does not consider about the overall frequency range performance. In fact, the bandwidth limitation of the design results mainly from the frequency dependence of  $X_s$  and  $X_m$ . In order to illustrate the  $X_s$  and  $X_m$  change with respect to frequency, we build the model for the two stubs by the aid of transmission line theory. Although the model is not accurate, it can help us to visualize the frequency variation.

The center frequency  $f_0$  is set at 2GHz. In Figure 4.3, the microstrip stub shows the property of shorted circuit at  $f_0$  and its odd multiples, and open circuit at its even multiples. Oppositely, in Figure 4.4, the slotline cavity shows the property of open circuit at  $f_0$  and its odd multiples, and shorted circuit at its even multiples.

According to Equation (4-2), we get the value of  $X$  with respect to frequency, as shown in Figure 4.5. By examining  $X_m$  and  $X$  simultaneously, we can see the microstrip stub and the slotline cavity really provide mutual cancellation among the whole frequency range but they can not be canceled exactly since  $X_m$  changes with frequency much faster than  $X$ . Therefore impedance bandwidth limitation is due to this fact.

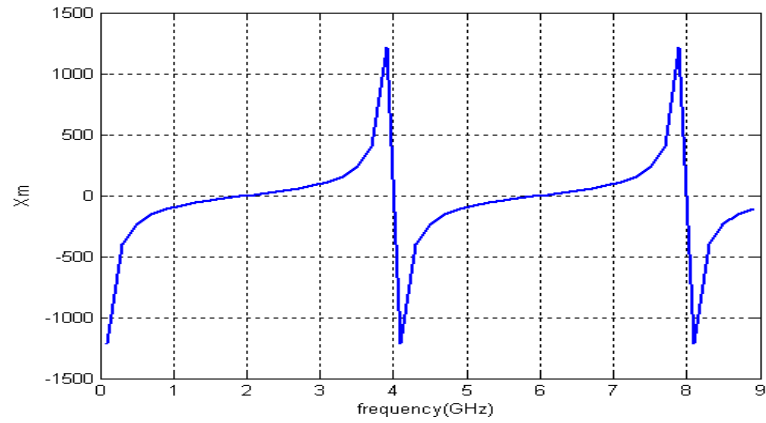


Figure 4.3 Reactance  $X_m$  of the microstrip stub

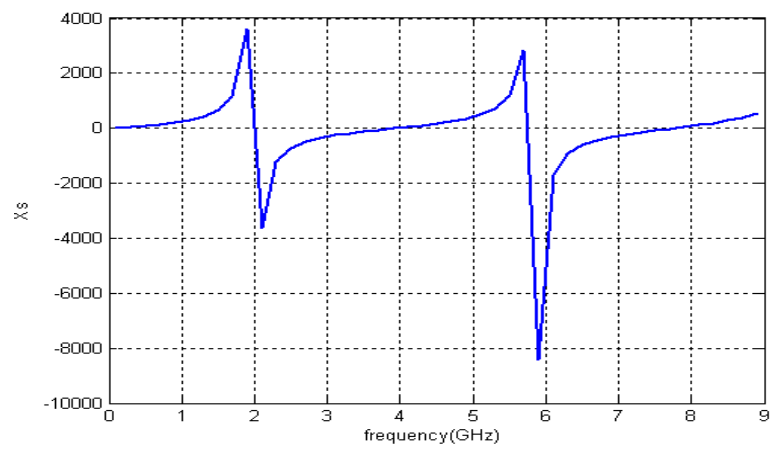


Figure 4.4 Reactance  $X_s$  for slotline cavity

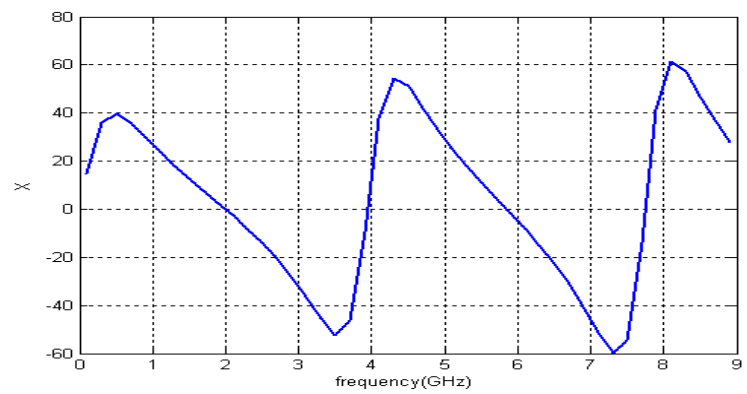


Figure 4.5 Reactance  $X$

The key point of our approach is to make the two resonators resonant at two different frequencies. Let the resonant frequency of microstrip line stub  $f_m > f_0$ . For

example,  $f_m = 3\text{GHz}$ . It can be predicted  $X_m$  will have the spike at about 6GHz and the value at the neighborhood of 4GHz will be quite small instead of a high spike shown in Figure 4.3. At the same time, let the resonant frequency of slotline cavity  $f_s < f_0$ . For example,  $f_s = 1\text{GHz}$ . It can be predicted  $X$  will have the spike at the neighborhood of 2GHz and the value at 4GHz will be quite small instead of a low valley shown in Figure 4-5. In this way, the lowest  $S_{11}$  close to zero at  $f_0$ , is sacrificed to get wider bandwidth among the overall frequency range.

The above discussion is based on uniform transmission line theory, while the radial microstrip stub and circular slotline cavity are nonuniform. To be more persuasive, we use CST simulation results to illustrate. Moreover, in order to figure out the effect of the parameter  $R_{rad}$  and  $D_s$  on the impedance performance individually, we did the CST simulation for the transition part by varying one parameter and fixing other parameters at constant values.

1) Diameter of the circular slotline cavity  $D_s$  changes

Rogers RO3003 with  $\epsilon_r = 3.0$   $h = 0.762\text{mm}$  is selected. In Figure 4.6,  $R_{rad}$  is fixed at 12.2 mm, corresponding to resonant frequency of the microstrip stub at 4GHz;  $D_s$  varies at the three values, 31.2mm, 14.9mm, 9.5mm (resonant at 2GHz, 4GHz, 6GHz respectively).

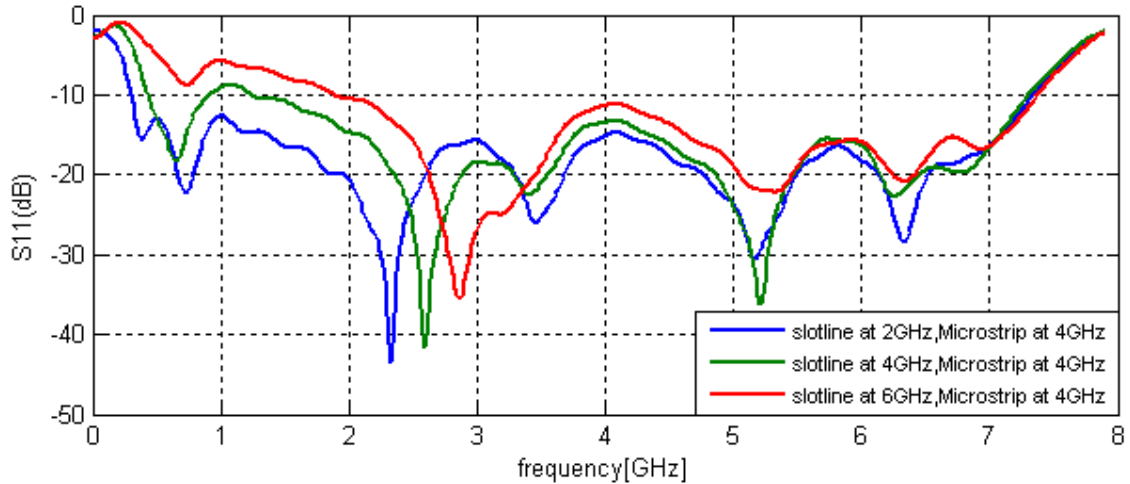


Figure 4.6 Reflection coefficient  $S_{11}$  (microstrip stub is resonant at 4GHz)

## 2) Radius of the radial microstrip stub $R_{rad}$ changes

In Figure 4.7,  $D_s$  is fixed at 14.9 mm, corresponding to resonant frequency of slotline cavity at 4GHz;  $R_{rad}$  varies at the three values, 24.7mm, 12.2mm, 8.1mm (resonant at 2GHz, 4GHz, 6GHz respectively).

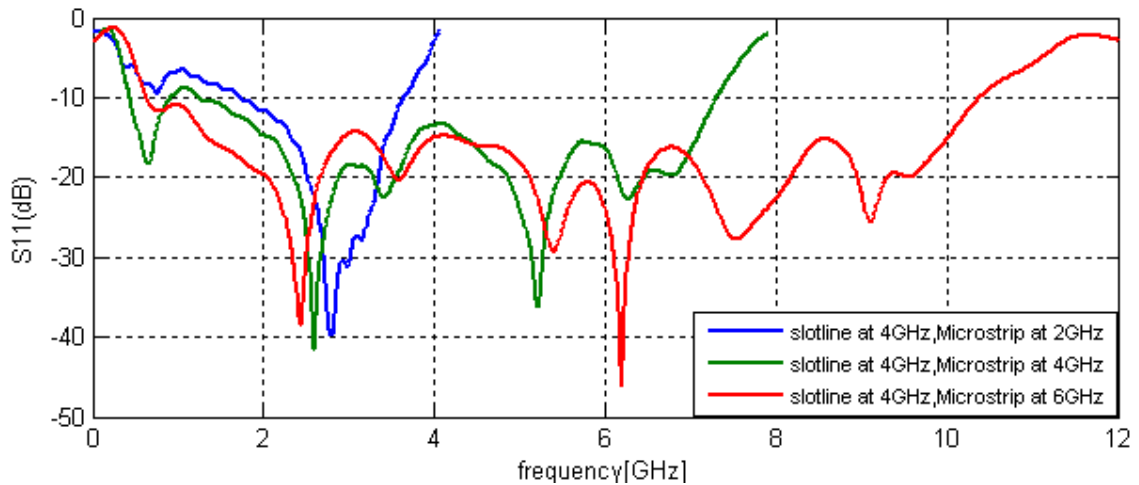


Figure 4.7 Reflection coefficient  $S_{11}$  (slotline cavity is resonant at 4GHz)

We really find that there is potential to get wider impedance bandwidth if the microstrip stub and slotline cavity are resonant at the same frequency (see the blue curve in Figure 4.6).

Moreover, there are more information expressed in Figure 4.6 and Figure 4.7.

Higher cutoff frequency of the transition part is totally determined by the length of the microstrip radial stub  $R_{rad}$ , or in other word by the resonant frequency of the microstrip radial stub. The lower cutoff frequency is dependent on two resonant frequencies of slotline cavity and microstrip stub.

#### 4.5 Parameter sweep

In order to find the optimal resonant frequency pair, parameter sweep is applied. In the There are 80 combinations totally.  $D_s$  varies from 5mm to 50mm with interval of 5mm.  $R_{rad}$  varies from 7.5mm to 25mm with interval of 2.5mm.

As it is shown in Figure 4.8, the maximum fractional impedance bandwidth is 30. It corresponds  $D_s=35\text{mm}$ ,  $R_{rad}=20\text{mm}$ . There is some deviation from black line which presents the track of microstrip stub and slotline cavity resonant at the same frequency.

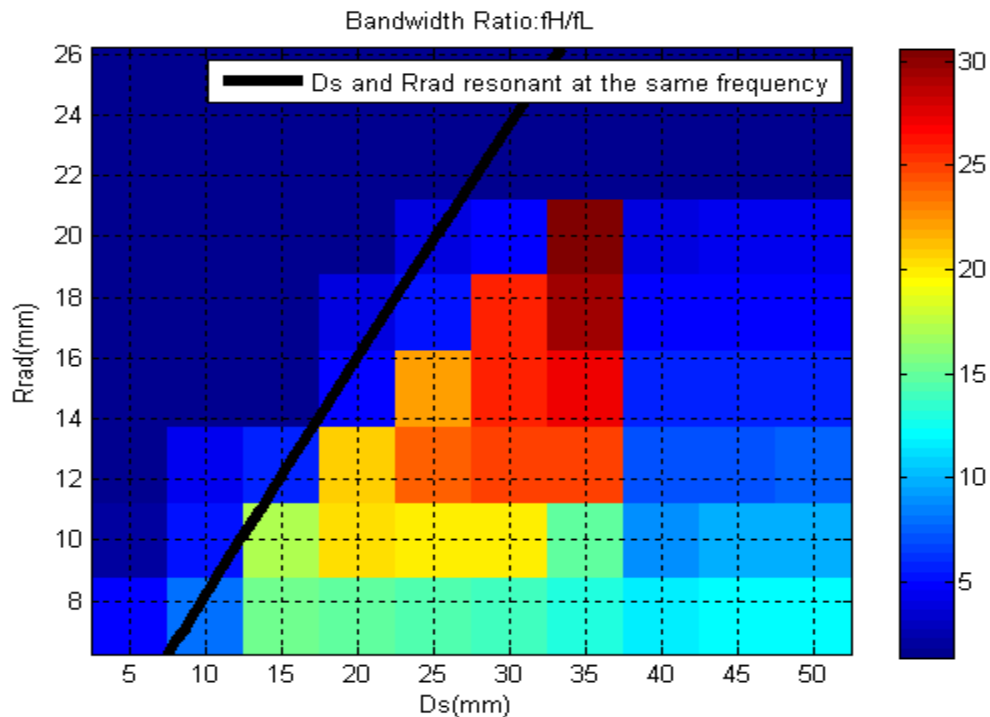


Figure 4.8 Fractional impedance bandwidth in regard to  $D_s$  and  $R_{rad}$

## 4.6 Conclusion

The radial microstrip stub and circular slotline cavity is used in the transition design for its wide impedance bandwidth. Traditionally, we design the size for two parts by making both of them resonant at the same center frequency. By observing the circuit model, we found that when they resonant at different frequency, especially the slotline cavity resonant at lower frequency and microstrip stub at higher frequency, the impedance bandwidth can greatly improved. Moreover, slot cavity diameter  $D_s$  impacts the lower frequency range a little bit while microstrip radial stub radius  $R_{rad}$  impacts the higher cutoff frequency significantly.

## CHAPTER V

### FINAL VIVALDI ANTENNA DESIGN

In the previous chapters, we have figured out the effect of the antenna parameters, substrate dielectric constant  $\epsilon_r$ , thickness  $h$ , curvature opening rate  $R$ , the radius of microstrip stub  $R_{rad}$  and diameter of slotline cavity  $D_s$  on antenna performance. Based on these findings and conclusions, we aim at designing a Vivaldi antenna with ‘optimal’ performance with respect to both impedance bandwidth and gain bandwidth.

#### 5.1 Design parameters

The final Vivaldi antenna is designed for 1 to 16 GHz at center frequency  $f_0 = \sqrt{f_1 f_2} = \sqrt{1 * 16} = 4GHz$ . To meet the goal of a broadband antenna both gain- and impedance, the parameters chosen based on the newly gained knowledge as well as fabrication issues requirement are provided as follows:

It is implemented on a Rogers RT5880 substrate with  $\epsilon_r=2.2$ , and thickness  $h=0.508$  mm. The Vivaldi antenna overall size is  $L=240$ mm, width  $W=120$ mm.  $W_0=100$ mm,  $L_0=200$ mm. The opening rate  $R$  is chosen  $0.015$ mm<sup>-1</sup> as a tradeoff between gain bandwidth and impedance bandwidth.  $D_s = 38$ mm which corresponds to the resonant frequency of slotline cavity at 1.8GHz, while  $R_{rad} = 7$ mm which corresponds to the resonant frequency of microstrip stub at 10GHz.

The slotline width at the beginning section is chosen as  $W_{sl} = 0.5\text{mm}$ . The selection is somewhat arbitrary and in this case it was made in order to have a low value of  $Z_{0s}$  for ease of transition to the microstrip input section while still being wide enough for accurate fabrication using standard PCB processes. The value of corresponding slotline impedance  $Z_{0s}$  is calculated by following formulas:

In this case, where the parameters satisfy

$$\begin{aligned} 2.2 \leq \varepsilon_r \leq 3.8 \\ 0.0015 \leq \frac{W_{sl}}{\lambda_0} \leq 0.075 \end{aligned} \quad (5-1)$$

the slot line impedance is <sup>[34]</sup>

$$\begin{aligned} Z_{0s} = & 60 + 3.69 \sin\left[\frac{(\varepsilon_r - 2.22)\pi}{2.36}\right] + 133.5 \ln(10\varepsilon_r) \sqrt{\frac{W_{sl}}{\lambda_0}} \\ & + 2.81[1 - 0.011\varepsilon_r(4.48 + \ln \varepsilon_r)] \left(\frac{W_{sl}}{h}\right) \ln\left(100 \frac{h}{\lambda_0}\right) \\ & + 131.1(1.028 - \ln \varepsilon_r) \sqrt{\frac{h}{\lambda_0}} + 12.48(1 + 0.18 \ln \varepsilon_r) \frac{W_{sl}}{h\sqrt{\varepsilon_r - 2.06 + 0.85(W_{sl}/h)^2}} \end{aligned} \quad (5-2)$$

The  $\lambda_0$  in the formula denotes the free space wavelength corresponding to center frequency  $f_0$ . For the desired antenna, the calculated values of  $Z_{0s}$  is  $109 \Omega$ .

As presented in Chapter 4, to get perfect impedance match for maximum power transition, slotline cavity and the microstrip stub reactance should be canceled. So,

$$Z_{0m} = n^2 Z_{0s} \quad (5-3)$$

where,

$$\begin{aligned}
n &= \cos 2\pi \frac{h}{\lambda_0} u - \cot(q_0) \sin 2\pi \frac{h}{\lambda_0} u \\
q_0 &= 2\pi \frac{h}{\lambda_0} u + \operatorname{tg}^{-1}\left(\frac{u}{v}\right) \\
u &= \left[\varepsilon_r - \left(\frac{\lambda_0}{\lambda_s}\right)^2\right]^{1/2} \quad v = \left[\left(\frac{\lambda_0}{\lambda_s}\right)^2 - 1\right]^{1/2}
\end{aligned} \tag{5-4}$$

and

$$\lambda_s = \lambda_0 \left(1.045 - 0.365 \ln \varepsilon_r + \frac{6.3(W_{sl}/h)\varepsilon_r^{0.945}}{238.64 + 100W_{sl}/h} - \ln \frac{h}{\lambda_0} \left[0.148 - \frac{8.81(\varepsilon_r + 0.95)}{100\varepsilon_r}\right]\right) \tag{5-5}$$

where  $\lambda_s$  is the wave length in slotline at center frequency  $f_0$ . Here the calculated values  $u = 0.99$ ,  $v = 0.47$ ,  $q_0 = 1.17$ ,  $n = 0.9813$  and the characteristic impedance of the microstrip at the cross plane  $Z_{0m} = 105.46\Omega$ , corresponding to a microstrip line width  $W_{ms} = 0.40\text{mm}$  which is calculated according to (5-6) [35]. Similarly, to make the feeding match to  $50\Omega$  coaxial SMA connector, the microstrip line width at the input section  $W_{ms0}$  is set at  $1.78\text{mm}$ .

$$\begin{aligned}
Z_{ms} &= \frac{120\pi}{\sqrt{\varepsilon_{eff}}} \left[ \frac{W_{ms}}{h} + 1.95 \left(\frac{W_{ms}}{h}\right)^{0.172} \right]^{-1} \\
\varepsilon_{eff} &= 1 + \frac{\varepsilon_r - 1}{2} \left[ 1 + \frac{1}{\sqrt{1 + 10h/W_{ms}}} \right]
\end{aligned} \tag{5-6}$$

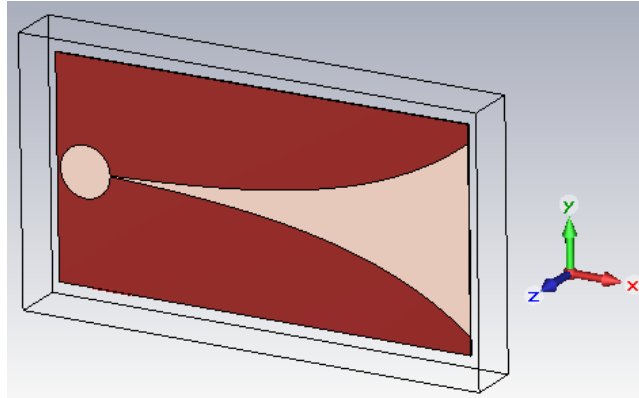


Figure 5.1 Final antenna modeled by CST

## 5.2 CST simulation results

The optimal antenna with the above parameter configuration is modeled and simulated under CST MWS.

Table5-1: simulation settings in CST MWS

| Feature           | Setting   |
|-------------------|---|
| Mesh Type         | hexahedral  |
| Mesh accuracy     | 20 lines per wavelength   |
| Port              | Waveguide port:10Wms0*5h  |
| Frequency         | 0~16GHz   |
| Solver Type       | Transient solver  |
| Solver accuracy   | -30dB   |
| Excitation signal | Gaussian with the spectrum from 0 to16GHz   |
| Field monitor     | E field at different frequency and at certain time duration<br>Far field at 0~16GHz with step of 0.2GHz |
| Probe             | E field at ( $\Phi=90^\circ$ $\theta=0^\circ$ Radius=5000m),farfield                                    |
| Outputs           | S parameter, E field, radiation pattern, signal at probe  |

### 5.2.1 Impedance bandwidth

The impedance bandwidth is counted in terms of the -10dB  $S_{11}$  as mentioned in Table1. As it is shown in Figure 5.2, the impedance bandwidth of the optimal Vivaldi antenna is from 1.46 GHz to 15GHz, and the fractional one is over 10:1.

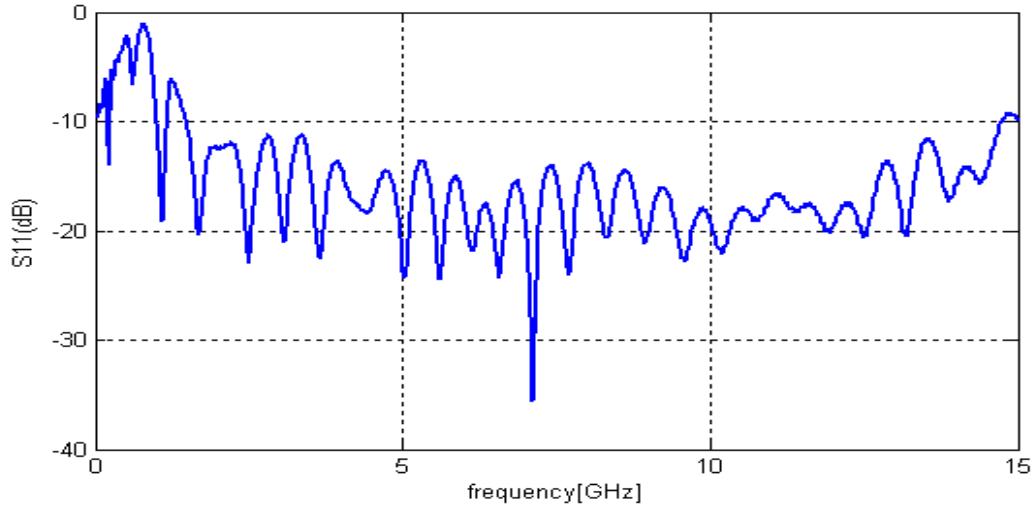


Figure 5.2 Simulated S11 of the final design

### 5.2.2 E field

The E field distribution pattern is similar in terms of frequency. Here, we take E field at frequency 4,8,12 GHz as example. From Figure 5.3, we can see that the excitation signal propagates from the input port through the transition of microstrip to slotline, and then radiates from the taper curve into free space. It is noted that the E field intensity along microstrip line and the tapered curvature is very strong while it is quite weak around the slotline cavity. Therefore, at some extent, the effect of slotline on the antenna performance is less sensitive than the microstrip and tapered curvature which is consistent with the conclusion in Chapter4.

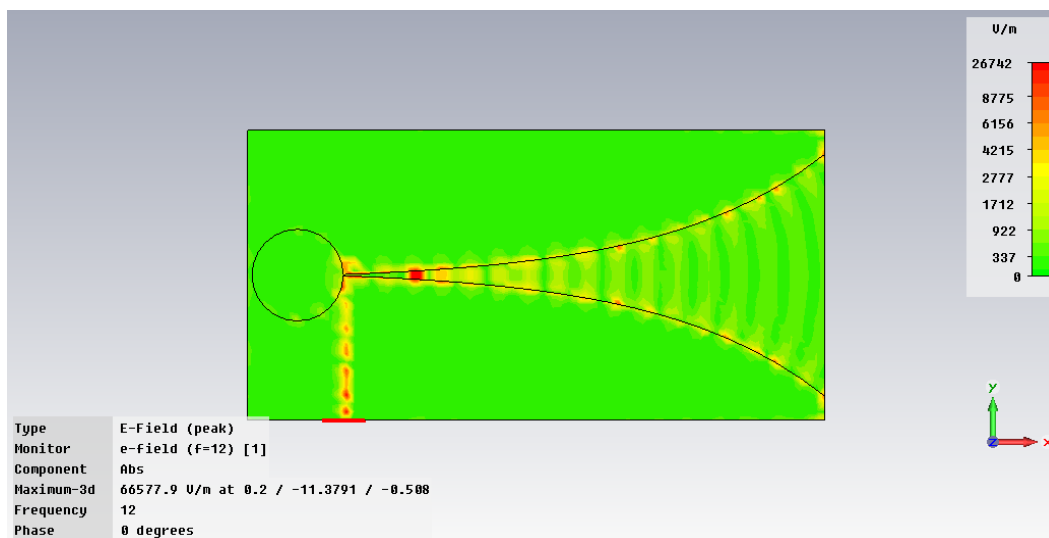
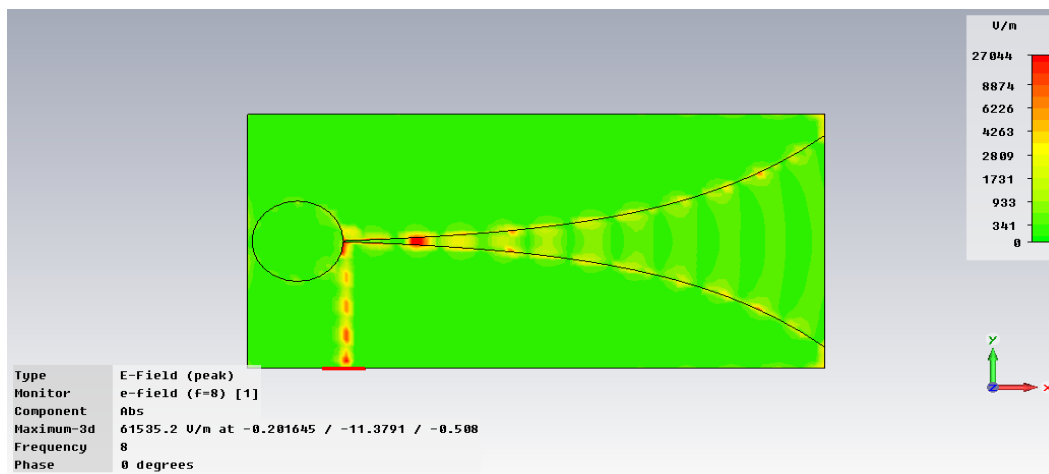
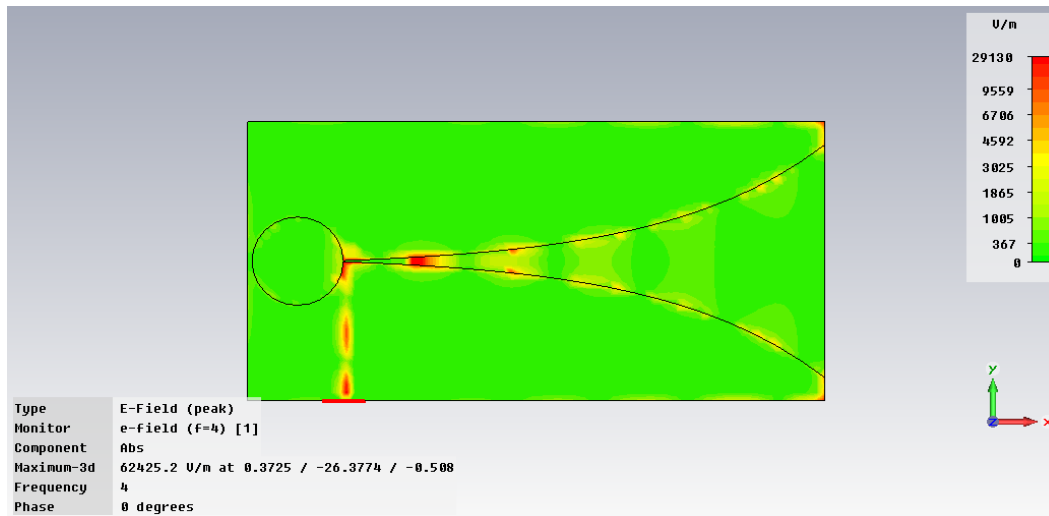


Figure 5.3 Simulated E field of the final design

a)f=4GHz b)f=8GHz c)12Ghz

### 5.2.3 Radiation pattern

Radiation pattern at frequency of 8 GHz is plotted with the polar plots in the Figure 5.4. It shows that the Vivaldi antenna is an end-fire radiating type of antenna. This further agrees with the theory as discussed in the literature. The principal direction of radiation (main lobe) is in the positive X direction.

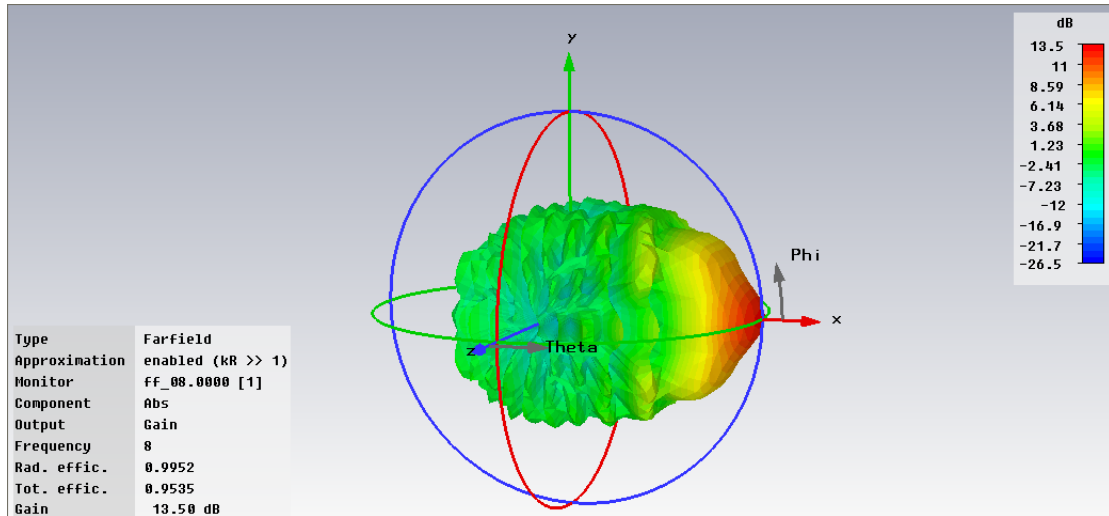


Figure 5.4 Simulated radiation pattern (f=8GHz) of the final design

Considering the main lobe in both cases, the E/H-plane is the plane containing the E/H-vector and passing through the origin. Thus the XY plane ( $\theta=90^\circ$ ) is the E-plane while the XZ plane ( $\phi=0^\circ$ ) is the H-plane. The E-plane and H-plane cuts for the frequencies of 4, 8 and 12 GHz are shown below. The plots shown below are for the total absolute gain in dB of the antenna at the above mentioned frequencies. It is seen that the gain is clearly a function of frequency and the radiation pattern does not split up at the 4, 8 and 12 GHz since the main lobe keeps at the direction of ( $\theta=90^\circ, \phi=0^\circ$ ) for all the three frequency points.

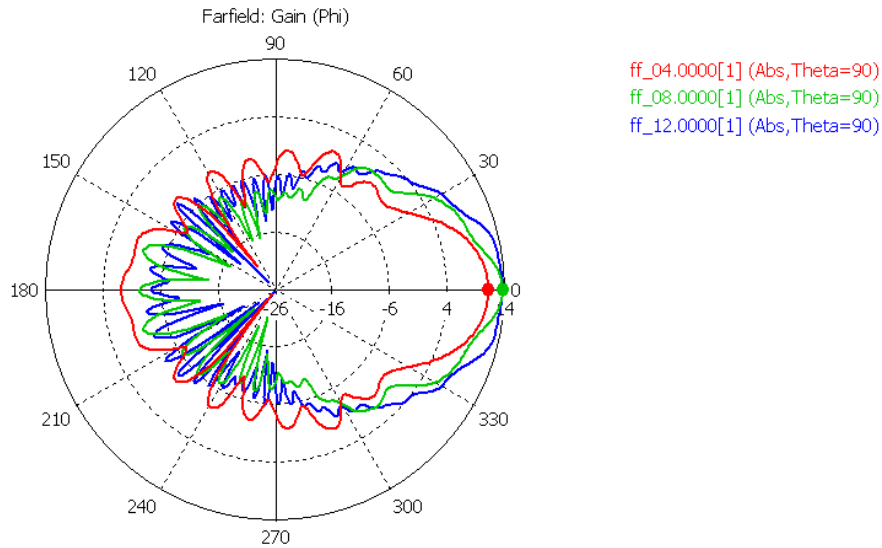


Figure 5.5 Radiation pattern: E plane at  $f=4,8,12$  GHz

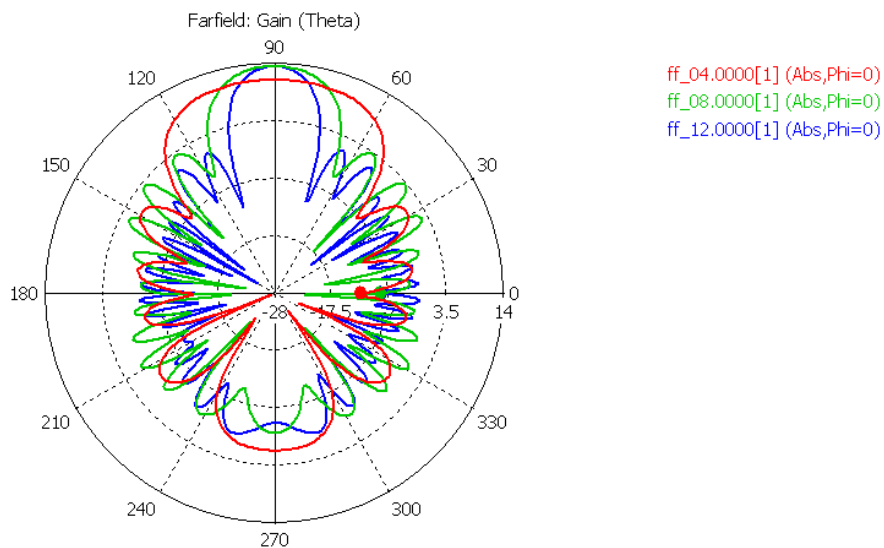


Figure 5.6 Radiation pattern: H plane at  $f=4,8,12$  GHz

### 5.2.4 Gain bandwidth

Three discrete frequencies only give three samples. In order to accurately determine the gain bandwidth, we plot the maximum gain pattern of all the directions and the gain at the direction of  $(\theta=90^\circ, \phi=0^\circ)$  among the frequency range of 0~16GHz. In Figure 5.7, the maximum gain pattern is almost the same as the gain pattern at the ‘supposed’ main lobe direction and both of them meet or exceed 3dB at the frequency range of

1.2GHz to 12GHz, which indicates there is no split within the frequency range. Therefore, both impedance bandwidth and gain bandwidth have 10:1 fractional bandwidth.

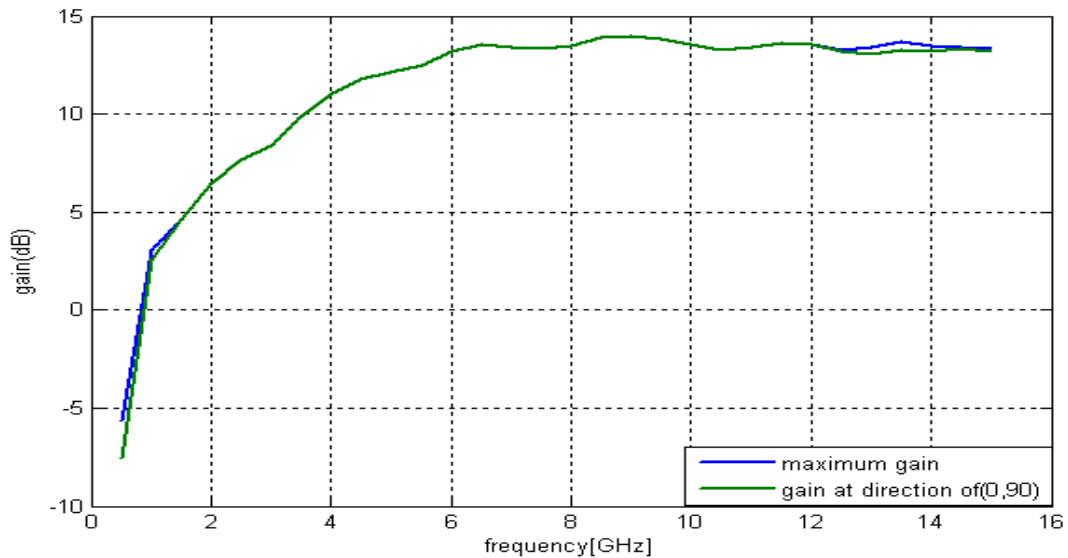


Figure 5.7 Simulated gain of the final design

### 5.2.5 Impulse response

A UWB antenna is characterized not only in the frequency domain but also in time domain. The performance of an UWB antenna can often be most advantageously described with descriptors to time domain such as impulse response.

As presented in Table 2.1, the input signal excited at the port is Gaussian function with the spectrum from 0 to 16GHz. The probe is placed at the point where Radius=5000m Phi=90° theta=0°. It is the main lobe direction and also satisfy far field distance. The signal itself and its derivation with respect to time in time domain are shown in Figure 5.8.

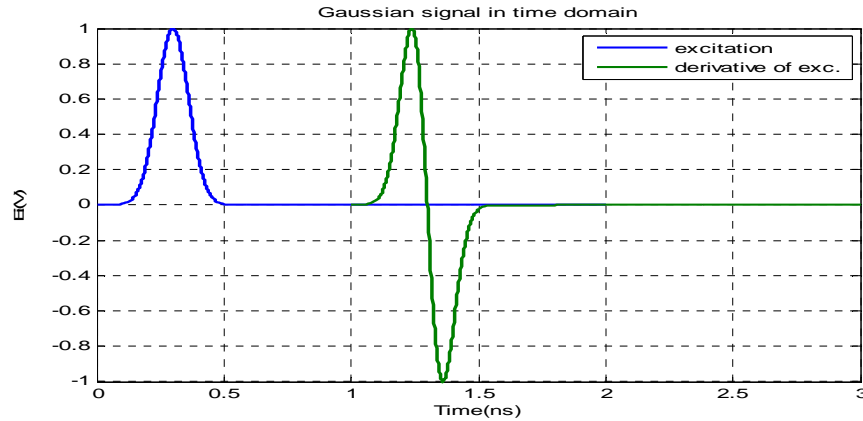


Figure 5.8 Excitation signal and its derivation

Because of derivative characteristics of antennas during the radiation <sup>[1]</sup>, the received impulse is ideally equal to the derivation of the excitation signal. Usually, for UWB antenna, the received signal shows some waveform distortion in the form of some ‘chirp’ due to the dispersion. Therefore, the impulse response is also a very importance indicator of the Vivaldi antenna as UWB antenna performance.

The radiated impulse signal at the main lobe direction of the final design is plotted in Figure 5.9. It really shows the ‘chirp’, however, it is slight and acceptable.

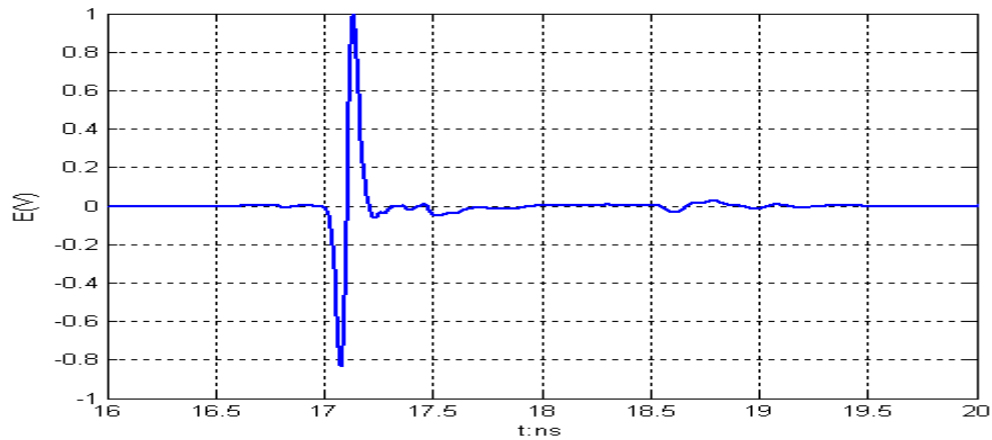


Figure 5.9 Radiated impulse at main lobe direction(normalized)

## CHAPTER VI

### VIVALDI ANTENNA MEASUREMENT

The parameters that often best describe an UWB antenna's characteristics are the impedance, pattern, gain, directivity, impulse response, etc. Testing the fabricated antenna's characteristics forms one of the most important activities in the whole process. In this chapter, we are going to measure those parameters of the optimal antenna after fabrication in order to verify the antenna practical performance.

#### 6.1 Test setup

The fabricated optimal Vivaldi antenna to be measured is shown in Figure 6.1.

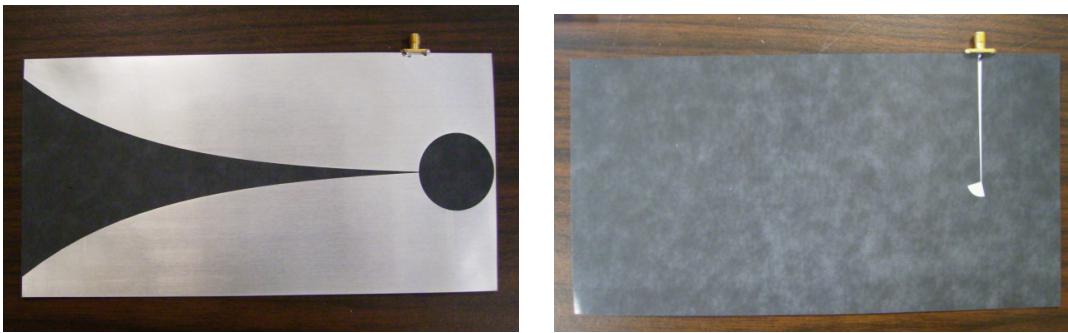


Figure 6.1 Fabricated antenna a) front view b)back view

In order to avoid surrounding environment interference, the testing is performed inside an anechoic chamber having walls that are covered with RF absorbers which provide a reflection coefficient of -40dB at normal incidence at frequencies as low as 100MHz. Agilent Network Analyzer 8719ET having operational frequency range of 50 MHz to 13.5GHz is applied in the following measurements.

## 6.2 Reflection measurement

Before the measurement, the Port1, reflection port of the Network Analyzer was calibrated to the input of the antenna (or end of the cable) over the 1-13.5GHz frequency range using SOLT method. The antenna under test was placed inside the anechoic chamber. The reflections from the antenna at each of these frequency points were obtained and plotted in Figure 6.2. There are two spikes at frequency region (10~12GHz) compared to the simulated result. However, they are below -10dB and acceptable.

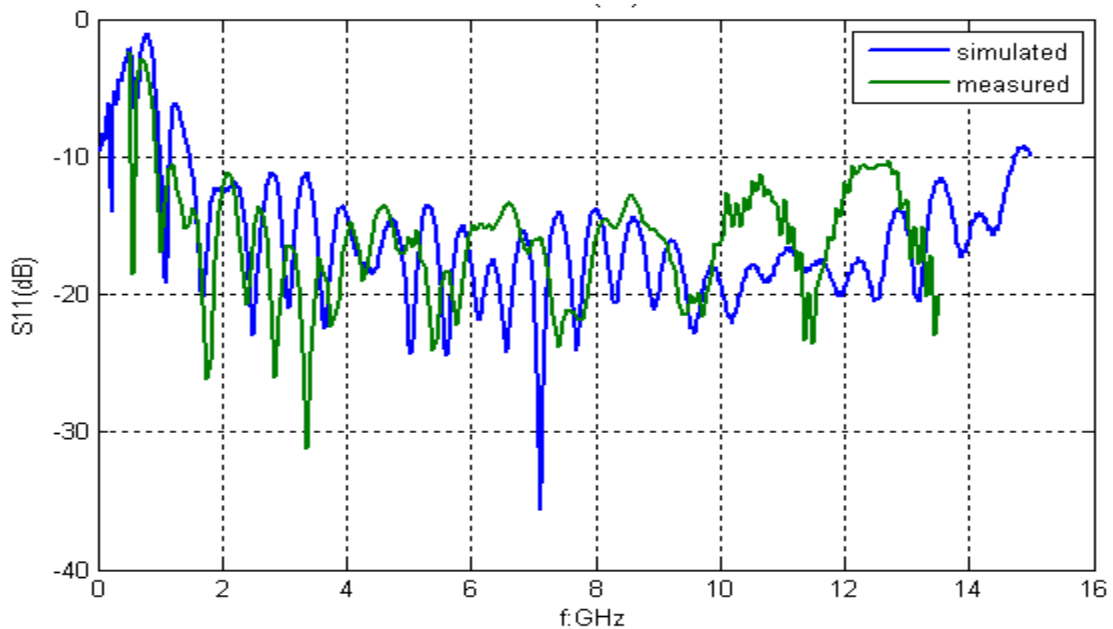


Figure 6.2  $S_{11}$  of the final design: Measured VS simulated

## 6.3 Gain measurement

The most important indicator that describes the performance of an antenna is the gain. Usually, there are two basic methods that can be used to measure the gain: absolute-gain and gain-transfer (or gain-comparison) measurements. The absolute-gain method requires no a priori knowledge of the gains of the antennas and gain-transfer must be used in conjunction with standard gain antennas. Here, we choose the absolute-gain method.

In the measurement, there are two identical antennas, one used for transmitting and the other one used for receiving. Assume that the transmitting and receiving are matched to their respective lines or loads and the polarization of the receiving antenna is polarization-matched to the incident wave. The reflection and polarization-matched antennas are also aligned for maximum directional radiation and reception. Then, the ratio of the received to the input power is represented by<sup>[35]</sup>

$$\frac{P_r}{P_t} = \left(\frac{\lambda}{4\pi R}\right)^2 G_{0t} G_{0r} \quad (6-1)$$

where,  $P_t$  is the input power at the terminals of the transmitting antenna;

$P_r$  is the power collected by the receiving antenna;

$G_{0t}$  is gain of the transmitting antenna;

$G_{0r}$  is gain of the receiving antenna;

$R$  is two antennas separation;

$\lambda$  is operating wavelength;

If the transmitting and receiving antennas are identical ( $G_{0t} = G_{0r}$ ), (6-1) reduces to

$$\begin{aligned} G(\omega) &= G_{0t} = G_{0r} = \frac{4\pi R}{\lambda} \sqrt{|S_{21}(\omega)|} \\ G(\omega)_{dB} &= \frac{1}{2} \left[ 20 \log_{10} \left( \frac{4\pi R}{\lambda} \right) + 10 \log_{10} \left( \frac{P_r}{P_t} \right) \right] \\ &= \frac{1}{2} \left[ 20 \log_{10} \left( \frac{4\pi R}{\lambda} \right) + S_{21}(\omega)_{dB} \right] \end{aligned} \quad (6-2)$$

The measured and simulated  $S_{11}$  are plotted in Figure 6.3. We can see they show good agreement.

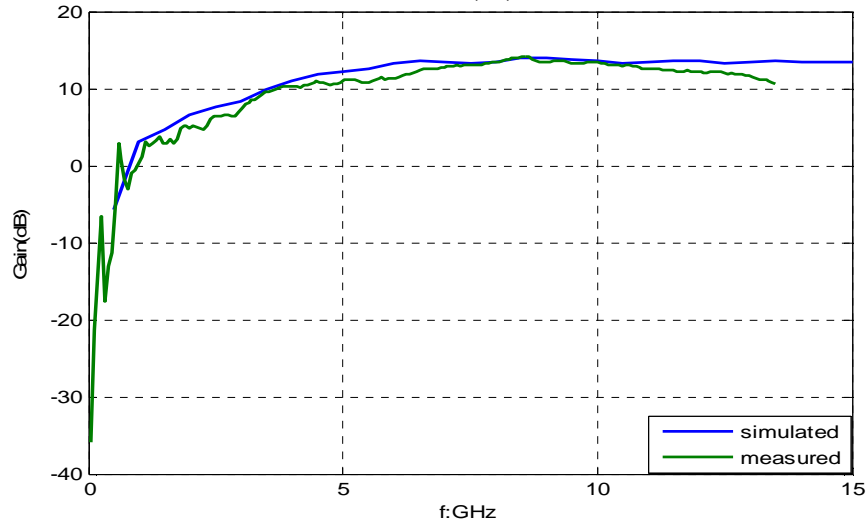


Figure 6.3 Gain of the final design: Measured VS simulated

#### 6.4 Impulse response measurement

Any fixed, linear, passive antenna, regardless of bandwidth, can be viewed as a linear time-invariant (LTI) system. Time-domain impulse response or equivalently, the complex frequency-domain transfer function is the fundamental quantity in the linear system analysis.

It is natural to compute such quantities from time domain data resulting from a fast rise-time source signal and measured directly with a high-speed digital sampling oscilloscope. While time-domain measurement system has matured greatly in recent years, frequency-domain automatic vector network analyzer exploit an enormous amount of work in calibration and de-embedding. Such a system is conceivable for a time-domain approach, but is not yet available<sup>[36]</sup>. Therefore, to get the impulse response, we make use of frequency domain data resulting from by Network Analyzer and then transform it into the time domain.

The transfer function of either of the identical antennas can be derived, and it is<sup>[36]</sup>

$$H(\omega) = \sqrt{\frac{2\pi R c_0}{j\omega} S_{21}(\omega) e^{j\omega R/c_0}} \quad (6-4)$$

Transfer the measured frequency domain data into time domain using FFT as well as advanced windowing techniques. The measured impulse response is obtained and shown in Figure 6.4 as well as the simulated result.

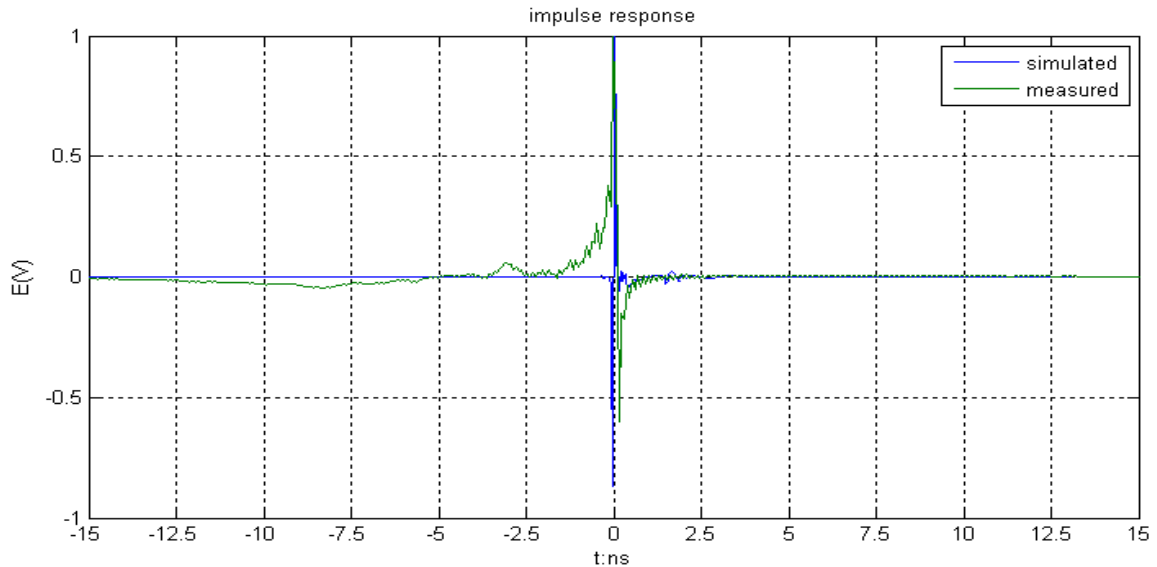


Figure 6.4 Impulse response of the final design: Measured VS simulated

In comparison to the simulated impulse response, the measured one shows more fluctuations. It can be explained by the fact that the Fourier Transform (or Inverse Fourier Transform) do not result in a perfect facsimile of the other. This is due to a number of factors, but limited frequency range and time-domain sampling rate are especially significant, since generally an antenna is not a low-pass (LP) system.

## CHAPTER VII

### CONCLUSION AND CONTRIBUTION

#### 7.1 Conclusion

A final Vivaldi antenna design with 10:1 bandwidth is achieved in terms of both impedance- and gain-bandwidth. Measurement results of the fabricated Vivaldi antenna show good agreements with the CST simulation results in terms of reflection coefficient, gain, and impulse response.

#### 7.2 Contribution

The contribution of this thesis can be concluded in to three aspects:

1. Divide the Vivaldi antenna into two parts

This has great advantages in finding the relationship between the antenna parameter and performance.

- Radiation pattern or directivity of the whole antenna dominantly depends on the taper curve part; while the transition part only affects the transmission efficiency.
- Impedance higher cutoff frequency is determined by the radial microstrip stub.
- Lower cutoff frequency lies on not only tapered curve, but also microstrip stub and slotline cavity.

2. Find the several ways to improve usable gain bandwidth by

- Using the substrate with lower dielectric constant.
- Using the substrate with thinner thickness.

3. Find the several ways to improve impedance bandwidth by
  - Making two resonators resonant at two separate frequencies, especially the slotline cavity resonant at lower frequency and microstrip stub at higher frequency,
  - Choosing proper opening rate by making tradeoff between two bandwidths.

## REFERENCES

- [1] Petr Cerny, Josef Nevrlý, Milos Mazanek, “Optimization of Tapered Slot Vivaldi Antenna for UWB Application”, *Applied Electromagnetics and Communications*, 2007. ICECom 2007. 19th International Conference on , 2007 , pp. 1-4.
- [2] P. J. Gibson, “The Vivaldi aerial” , *Proceedings of the 9th European Microwave Conference*, 1979, pp. 103-105.
- [3] R. Janaswamy, D. H. Schaubert, and D. M. Pozar, “Analysis TEM mode linearly tapered slot antenna” , *Radio Science*, Vol. 21, 1986, pp. 797–804.
- [4] T. A. Axness, R. V. Coffmann, B. A. Kopp, and K. W. O’Haver, “Shared aperture technology development” , *Johns Hopkins APL Tech.Dig.*, vol. 17, no. 3, pp. 285–294, 1996.
- [5] S. Balling, M. Hein, M. Hennhofer, G. Sommorkorn, R. Stephan, and R. Thoma, “Broadband dual polarized antenna arrays for mobile communication applications” , *Proc. 33rd Eur. Microw. Conf.*, Munich, Germany, Oct. 6–10, 2003, pp. 927–930.
- [6] A. A. Golovkov, V. B. Khaikin, E. Y. Golubeva, D. A. Kaliniko, B. A. Kiselev, and M. I. Sugak, “Wideband Vivaldi feed for a reflector radio telescope” , *Proc. URSI/IEEE XXVII Conv. RadioSci.*, Espoo, Finland, Oct. 2002, pp. 84–87.
- [7] J. A. N. Noronha, T. Bielawa, C. R. Anderson, D. G. Sweeney, S. Licul, and W. A. Davis, “Designing Antennas for UWB Systems” , *Microw. RF*, vol. 42, no. 6, pp. 53–61, Jun. 2003
- [8] W. H. Weedon, W. C. Chew, and P. E. Mayes, “A step frequency radar imaging system for microwave nondestructive evaluation” , in *Proc. PIER 28*, 2000, pp. 121–146.

- [9] E. Guillanton, J. Y. Dauvignac, C. Pichot, and J. Cashman, "A new design tapered slot antenna for ultra-wideband applications", *Microw.Opt. Technol. Lett.*, vol. 19, no. 4, pp. 286–289, 1998.
- [10] C. Pichot et al., "Recent nonlinear inversion methods and measurement system for microwave imaging", *Proc. IEEE Int. Workshop IST*, Stresa, Italy, May 14, 2004, pp. 95–99.
- [11] R. Q. Lee and R. N. Simons, "Effect of Curvature on Tapered Slot Antennas", *Antennas and Propagation Society International Symposium, AP-S. Digest, Vol. 1*, 1996, pp. 188-191.
- [12] Adrian T.Sutinjo and Edwin Tung, "The Design of A Dual Polarized Vivaldi Array", *Microwave Journal*, Sep 2004,09
- [13] J. P. Weem, Z. Popovic, and B. M. Notaros, "Vivaldi antenna arrays for SKA", *Antennas and Propagation Society International Symposium, Vol.1*, 2000, pp. 174-177.
- [14] R. Rajaraman, "Design of a Wideband Vivaldi Antenna Array for the Snow Radar", *Master thesis, The University of Kansas, India*, 2004.
- [15] Chao Deng and Yong-jun Xie, "Design of Resistive Loading Vivaldi Antenna", *IEEE Antennas and Wireless Propagation Letters, Vol. 8*, 2009
- [16] Alexander N. Sharp, Ross Kyprianou, "Vivaldi antennas: Wideband Radar Antennas Simulation and reality", *2007 IET International Conference on Radar Systems*, pp.1-5
- [17] Kai Fong Lee and Wei Chen, "Advances in Microstrip and Printed Antennas", *John Wiley and Sons*, 1997.
- [18] Homayoon Oraizi, Shahrokh Jam, "Optimum Design of Tapered Slot Antenna Profile," *IEEE Transactions on Antennas and Propagation, Vol.51, No.8, August 2003*
- [19] B. Schuppert, "Microstrip/slotline transitions: Modeling and experimental investigations", *IEEE Trans., Vol. MTT-36*, 1988, pp. 1272-1282.

- [20] Robert E. Collin, "Foundations for Microwave Engineering", The Institute of Electrical and Electronics Engineers, Inc., New York.
- [21] Kai Fong Lee, Wei Chen, "Advanced Microstrip and Printed Antennas", Wiley Series in Microwave and Optical Engineering, 1997
- [22] Adrian T. Sutinjo, Edwin Tung, "The Design of a Dual Polarized Vivaldi Array", Microwave Journal, September 2004.
- [23] Alexander N. Sharp, Ross Kyprianou, "Vivaldi antennas: Wideband Radar Antennas Simulation and reality", 2007 IET International Conference on Radar Systems pp.1-5
- [24] Chao Deng and Yong-jun Xie, "Design of Resistive Loading Vivaldi Antenna", IEEE Antennas and Wireless Propagation Letters, Vol.8, 2009
- [25] D.A. Burrell, J.T. Aberle, "Characterization of Vivaldi Antennas Utilizing a Microstrip-to Slotline", IEEE CNF, 1993, pp.1212-1215.
- [26] K.C Gupta, Ramesh Garg, Inder Bahl and Prakash Bhartia, "Microstrip Lines and Slotlines", Second Edition, Artech House Publisher, 2007, pp306-308, pp195.
- [27] Wadell, Brian C. "Transmission Line Design Handbook", Artech House, Inc. 1991.
- [28] Harry A. Atwater, "Microstrip Reactive Circuit Elements", IEEE Transaction on Microwave Theory and Techniques, Vol. MIT-31, No.6, June 1983.
- [29] Jerzy Chramiec, "Reactance of Slotline Short and Open Circuits on Alumina Substrate", IEEE Transaction on Microwave Theory and Techniques, Vol.37, No.10, June 1989
- [30] Yu-Chuan Su, Marek E. Bialkowski, "UWB Switched-Beam Array Antenna Employing UWB Butler Matrix", Proceedings of iWAT2008, Chiba, Japan
- [31] B. Schuppert, "Microstrip-slotline transitions: Modeling and experimental investigation", IEEE Trans. Microwave Theory, Vol.36, PP1272-1282, 1988.

- [32]P.Soltysiak and J.Chramiec, “Design of broadband transitions from microstrip to slotline”, Electronics letters,1994,Vol.30,No.4
- [33] Hans Schantz, “The Art and Science of Ultra wideband Antennas’’,2005 Artech House,Inc.
- [34]R.Janaswamy,D.H.Schaubert, “Characteristic Impedance of a Wide Slotline on Low-Permittivity Substrates’’,IEEE Transactions on Microwave Theory and Techniques, Vol.MTT-34,No.8,August1986
- [35]Constantine A.Balanis, “Antenna Theory Analysis and Design(second edition)’’, John wiley &Sons,Inc,1997
- [36]James S.McLean,Robert Sutton,Armando Medina,Heinrich Foltz,Junfei Li, “The Experimental Characterization of UWB Antennas via Frequency-Domain Measurements’’,IEEE Antennas and Propagation Magazine, Vol.49, No.6, December 2007.
- [37] <http://www.ansoft.com/products/hf/hfss>
- [38] <http://www.cst.com/Content/Products/MWS/Overview.aspx>

## BIOGRAPHICAL SKETCH

Fang Chen was born in P.R.China in Sep.1983 as the daughter of Huasao Chen and Min Wang. She received her bachelor, Master's Degree in Electronics and Information College of Northwestern Polytechnical University, Xi'an, Shaanxi, P.R.China in 2006 and 2009 respectively. Her master research in China focused on the electromagnetic countermeasure, radar system modeling and simulation. In August 2008, she joined Master program in Electrical Engineering Department of the University of Texas-Pan American. Her research fields include UWB antenna design and simulation, electromagnetic computation, and radar imaging.